

24 Abstract

25 During clathrin-mediated endocytosis in eukaryotes, actin assembly is required to
26 overcome large membrane tension and turgor pressure. However, the molecular
27 mechanisms that enable the actin machinery to adapt to varying membrane tension
28 remain unclear. Here, we used quantitative microscopy to determine that, upon
29 increased membrane tension, the endocytic actin machinery of fission yeast cells
30 rapidly adapts. We also demonstrate that cells rapidly reduce their membrane
31 tension using three parallel mechanisms. In addition to using their cell wall for
32 mechanical protection, yeast cells disassemble eisosomes to buffer moderate
33 changes in membrane tension on a minute time scale. Meanwhile, a temporary
34 reduction of the rate of endocytosis for 2 to 6 minutes, and an increase in the rate of
35 exocytosis for at least 5 minutes allow cells to add large pools of membrane to the
36 plasma membrane. Our study sheds light on the tight connection between membrane
37 tension regulation, endocytosis and exocytosis in yeast, which are likely conserved
38 among eukaryotes.

39
40

41 Introduction

42 During clathrin-mediated-endocytosis (CME), the cell plasma membrane
43 undergoes a dramatic change in topology to form an invagination that is
44 subsequently pinched off into a vesicle. During this process, the endocytic machinery
45 has to overcome the forces produced by membrane tension and the osmotic
46 pressure that oppose membrane deformation and engulfment. In yeast cells, these
47 resisting forces are particularly large because their internal turgor pressure is high,
48 ranging from ~0.6 MPa for *Saccharomyces cerevisiae* to more than 1 MPa for
49 *Schizosaccharomyces pombe* (Davi et al., 2018; Minc et al., 2009; Schaber et al.,
50 2010). Consequently the formation of a vesicle requires several thousands of pN
51 (Dmitrieff and Nédélec, 2015; Ma and Berro, 2020).

52 Previous studies have shown that actin dynamics are required for productive
53 endocytosis in yeast (Aghamohammadzadeh et al., 2014; Basu et al., 2013; Carlsson
54 and Bayly, 2014; Lacy et al., 2018; Palmer et al., 2015) and in mammalian cells
55 when membrane tension is high (Aghamohammadzadeh and Ayscough, 2009;
56 Boulant et al., 2011; Hassinger et al., 2017), or when membrane scission proteins
57 are absent (Ferguson et al., 2009). Actin assembly at the endocytic site is believed to
58 provide the forces that overcome turgor pressure and membrane tension to deform
59 the plasma membrane, but the precise mechanisms of force production remain
60 unknown. We also lack a quantitative understanding of the regulation of actin
61 dynamics in response to membrane tension and turgor pressure changes. We expect
62 that a better quantitative characterization of this response will allow us to infer the
63 molecular mechanisms of force production and force sensing during clathrin-
64 mediated endocytosis.

65 In this study, we applied hypotonic shocks to fission yeast cells to determine
66 how the actin machinery responds to increased membrane tension and turgor
67 pressure during clathrin-mediated endocytosis. After a hypotonic shock, the
68 difference in osmolarity inside and outside the cell instantaneously increases the
69 turgor pressure and the membrane tension. Since cell membranes are virtually

70 unstretchable, yeast cells must rapidly adapt their membrane tension while they let
71 water flow inward to equilibrate their cytosol osmolarity to the new environment
72 (Hohmann, 2015, 2002; Suescún-Bolívar and Thomé, 2015).

73 The mechanisms by which membrane tension is regulated are not fully
74 understood. The yeast cell wall is believed to buffer abrupt changes in turgor
75 pressure thanks to its high stiffness of ~50 MPa (Atilgan et al., 2015). In addition,
76 similarly to mammalian cells' caveolae which change shape or disassemble in
77 response to increased membrane tension, yeast eisosomes can also disassemble
78 when cells without a cell wall, called protoplasts, are placed in low osmolarity media
79 (Kabeche et al., 2015; Parton et al., 2019; Sinha et al., 2011). However, it remains
80 unknown how eisosomes may regulate plasma membrane tension in intact cells, and
81 whether eisosomes disassembly directly influences cellular processes such as CME.

82 Fission yeast is an ideal model system to quantitatively study the regulation
83 mechanisms of membrane tension and its influence on the endocytic machinery.
84 First, because yeast turgor pressure is high, actin is required for CME. Second,
85 contrary to mammalian cells, yeast cells are devoid of any adhesion machinery or
86 actin cortex, which usually complicates membrane tension manipulation and result
87 interpretation. Last, quantitative microscopy methods developed in fission yeast are
88 able to uncover fine regulations of the endocytic machinery (Arasada and Pollard,
89 2011; Berro et al., 2010; Berro and Lacy, 2018; Berro and Pollard, 2014a, 2014b;
90 Chen and Pollard, 2013; Sirotkin et al., 2010).

91 To probe the contribution of each possible mechanisms of membrane tension
92 regulation and their influence on CME, we submitted yeast cells with or without a cell
93 wall to different hypotonic shocks. Using quantitative fluorescence microscopy, we
94 showed that, on the one hand, actin assembly adapts to increased membrane
95 tension to allow endocytosis to proceed, and, on the other hand, yeast cells rapidly
96 reduce their membrane tension by a) disassembling eisosomes, b) reducing their
97 rate of endocytosis and c) increasing their rate of exocytosis.

98 Results

99 **Clathrin-mediated endocytosis in wild-type walled cells is robust over a wide** 100 **range of chronic and acute changes in media osmolarity**

101 To monitor actin dynamics during clathrin-mediated endocytosis, we imaged
102 fission yeast cells expressing the actin filament crosslinking protein fimbrin (Fim1p)
103 tagged with a monomeric enhanced green fluorescent protein (mEGFP), hereafter
104 called Fim1p-mEGFP (Figure 1A, 1B and 1C). Fimbrin is a bona fide marker for
105 endocytosis in yeast since it has spatial and temporal co-localization with the
106 classical endocytic marker End4p (the fission yeast homolog of mammalian Hip1R
107 and budding yeast Sla2) during endocytosis (Figure 1D, 1E). Fimbrin's time of
108 appearance, disappearance, peak number of molecules and spatial localization
109 follows those of actin in wild-type and all mutants tested so far (Arasada et al., 2018;
110 Berro and Pollard, 2014b; Chen and Pollard, 2013; Sirotkin et al., 2010). Fimbrin is
111 the most abundant endocytic proteins that is fully functional when tagged with a
112 fluorescent protein at either N- or C-terminal, which makes it a more robust marker
113 for actin dynamics than tagged actin or actin-binding markers such as LifeAct or
114 calponin-homology domains, because they require over-expression which is difficult
115 to control precisely in fission yeast, and potentially creates artifacts (Courtemanche
116 et al., 2016; Suarez et al., 2015). We optimized our imaging protocols, and improved
117 tracking tools and temporal super-resolution alignment methods (Berro and Pollard,
118 2014a) to a) easily collect hundreds of endocytic events in an unbiased manner and
119 b) achieve high reproducibility between different samples, fields of view and days of
120 experiment (Figure 1F, 1G). These improvements in our quantitative microscopy
121 protocol have allowed us to detect small differences between mutants or conditions
122 that would be missed with previous methods. We confirmed that Fim1p accumulates
123 at endocytic sites for about 10 seconds, and then disassembles while the vesicle
124 diffuses away from the plasma membrane (Figure 1F, 1G) (Sirotkin et al., 2010; Skau
125 et al., 2011). As a convention, the peak of Fim1p is set to time 0 s and corresponds
126 to vesicle scission in intact wild-type cells (Berro and Pollard, 2014a, 2014b; Sirotkin
127 et al., 2010). In the rest of the paper, intact cells with a cell wall will be referred to as
128 "walled cells", and cells devoid of a cell wall will be referred to as "protoplasts".

129 We aimed to increase the tension of cells' plasma membrane by rapidly reducing
130 media osmolarity, referred to as acute hypotonic shock. To prevent artifacts due to
131 nutrient concentration changes, we supplemented Edinburgh Minimum Media
132 (EMM5S) with varying sorbitol concentrations (0 to 1.2 M). Before performing
133 hypotonic shocks, we exposed cells to this media for more than 15 minutes. In the
134 rest of the paper, we will refer to this experimental condition as steady state at X M or
135 chronic exposure to X M sorbitol, where X is the sorbitol concentration. To perform
136 acute hypotonic shocks, we used a microfluidic system to rapidly exchange the
137 steady state media with media containing a lower sorbitol concentration, hereafter
138 noted $\Delta P = -Y$ M where Y is the difference in media osmolarity (note that the pressure
139 P^* in Pascal is related to P in Molar as $P^* = P \cdot RT \sim 2.45 \cdot 10^6 \cdot P$, where R is the gas
140 constant and T the absolute temperature) (Figure 2A). For all tested osmolarities at
141 steady state in walled wild-type cells, we observed no significant difference in the
142 dynamics of fimbrin recruitment or disassembly, maximum molecule number or
143 endocytic patch movements (Figure 2B). Our results indicate that wild-type walled
144 cells have adaptation mechanisms for chronic exposure to a wide range of
145 osmolarities, which allows them to perform CME in a highly reproducible manner.

146 We then tested the robustness of the endocytic actin machinery when cells
147 experienced a hypotonic shock, which aimed to abruptly increase the tension of their
148 plasma membrane. To observe the highest possible effect, we imaged cells grown at
149 steady state in 1.2 M sorbitol and rapidly exchanged the media with a buffer free of
150 sorbitol (Figure 2A and 2E), therefore performing an acute hypotonic shock of $\Delta P = -$
151 1.2 M. Despite the high hypotonic shock, which represents a ~ 3 MPa drop in
152 pressure, CME proceeded quite similarly to steady state conditions (Figure 2C, 2D
153 and 2E). The maximum number of fimbrin proteins was the same before and after the
154 hypotonic shock, but fimbrin assembly and disassembly were $\sim 15\%$ faster after the
155 shock (Figure 2E).

156

157 **Eisosomes mitigate the response of the endocytic machinery to acute and** 158 **chronic changes in media osmolarity**

159 The robustness of the endocytic process under a wide range of chronic and acute
160 exposure to different media osmolarity suggests that fission yeast has mechanisms
161 that rapidly regulate plasma membrane tension. Previous studies proposed that
162 eisosomes, furrows at the inner surface of the plasma membrane, have a
163 mechanoprotective role under increased membrane tension in fungi, similar to the
164 protective role of caveolae in endothelial cells (Cheng et al., 2015; Kabeche et al.,
165 2015; Lo et al., 2016; Sens and Turner, 2006; Sinha et al., 2011). Because loss of
166 Pil1p, the core eisosome component, is sufficient to prevent eisosome assembly
167 (Kabeche et al., 2011; Olivera-Couto et al., 2011; Ziłkowska et al., 2011), we
168 repeated our experiments in cells lacking the gene coding for Pil1p (*pil1 Δ*) (Figure 3).

169 Dynamics of Fim1p during CME for wild-type and *pil1 Δ* walled cells at steady
170 state in media free of sorbitol were identical (Figure 3 Supplement 1). However, at
171 steady state in media with high sorbitol concentration, cells lacking eisosomes
172 recruited slightly fewer fimbrin molecules to endocytic patches than wild-type cells
173 (Figure 3A and B). The maximum number of Fim1p assembled at CME sites in *pil1 Δ*
174 cells in buffer containing 0.8 M and 1.2 M sorbitol was 10% and 17% lower,
175 respectively. Within the first two minutes of an acute hypotonic shock from 1.2 M
176 sorbitol to 0 M ($\Delta P = -1.2$ M), the maximum number of Fim1p increased by 30%, while
177 its timing was shortened by $\sim 30\%$ compared to steady-state (Figure 3C & 3D). Four
178 minutes after the hypotonic shock, the dynamics of fimbrin stabilized at its steady
179 state dynamics in 0 M sorbitol (Figure 3B & 3D). Overall, our data show that the
180 endocytic actin machinery in cells lacking eisosomes is more sensitive to acute and
181 chronic changes in media osmolarity than in wild-type cells.

182

183 **Eisosomes participate in the regulation of protoplasts' membrane tension** 184 **during hypotonic shocks**

185 The yeast cell wall plays a role in the maintenance of cell integrity under extreme
186 conditions, thanks to its high stiffness of ~ 50 MPa (Atilgan et al., 2015). We
187 hypothesized that the cell wall prevents large variations in membrane tension under
188 hypotonic shocks, which would explain why endocytosis in wild-type walled cells
189 remains virtually unchanged in the extreme conditions we tested (Figure 2E). Hence,
190 to exclude the effect of the cell wall, we reiterated our experiments using protoplasts
191 instead of intact cells.

192 First, we characterized how the removal of the cell wall affects eisosomes'
193 reorganization and CME. We used a protocol that allowed us to manipulate
194 protoplasts for up to ~ 1 hour after their formation, since they remain void of cell wall
195 for about 3 hours (Flor-Parra et al., 2014). Because protoplasts are more fragile than

196 walled cells, they were prepared in media containing 0.25 to 1.2 M sorbitol to balance
197 turgor pressure and prevent cells from bursting (Basu et al., 2013; Kabeche et al.,
198 2015; Stachowiak et al., 2014), and were imaged ~15 minutes later, once they
199 reached steady state.

200 Our data show that endocytic patches and eisosomes in protoplasts at steady
201 state in 1.2 M sorbitol are qualitatively similar to those in walled cells (Figure 4A) and
202 the cellular concentration of Pi1p is the same in both conditions (Figure 4 –
203 Supplement 1A). However, the surface area of the protoplasts' plasma membrane
204 covered by eisosomes decreased with decreasing media osmolarity at steady state
205 (Figure 4B and 4C), and correlated with increasing cell volume (Figure 4 –
206 Supplement 1B). This result confirms previous results (Kabeche et al., 2015) showing
207 that eisosomes are disassembled in media with low osmolarity and the disassembly
208 of eisosomes may reduce membrane tension.

209 To test whether membrane tension is indeed buffered by eisosomes, we
210 measured membrane tension using a micropipette aspiration assay (Figure 4D). At
211 steady state in 0.8 M sorbitol, the membrane tension was $4.5 \pm 1.4 \cdot 10^{-4} \text{ N}\cdot\text{m}^{-1}$ for wild-
212 type protoplasts and $3.9 \pm 1.3 \cdot 10^{-4} \text{ N}\cdot\text{m}^{-1}$ for *pil1Δ* protoplasts (Figure 4E). We then
213 repeated these measurements within 5 minutes after inducing a hypotonic shock of
214 $\Delta P = -0.2 \text{ M}$. We observed a 1.6-fold increase in membrane tension for wild-type
215 protoplasts ($7.3 \pm 2.1 \cdot 10^{-4} \text{ N}\cdot\text{m}^{-1}$) and a 4.5-fold increase for protoplasts lacking
216 eisosomes ($17.4 \pm 6.1 \cdot 10^{-4} \text{ N}\cdot\text{m}^{-1}$). This result demonstrates that eisosomes participate
217 in the adjustment of plasma membrane tension.

218 To confirm that eisosomes disassemble in protoplasts after a hypotonic treatment
219 (Kabeche et al., 2015), and quantitatively characterize this disassembly, we
220 measured the temporal evolution of the decrease in surface area covered by
221 eisosomes after an acute hypotonic shock of $\Delta P = -0.2 \text{ M}$ (Figure 4H and 4I).
222 Eisosomes disassembled rapidly after hypotonic shock, dropping to ~50% of the
223 surface area covered by eisosomes before the shock within 5 min, indicating a fast
224 response to counteract changes in membrane tension.

225

226 **CME in protoplasts is sensitive to chronic changes in osmolarity**

227 Endocytosis in wild-type protoplasts at steady state in medium containing 0.4 or
228 0.8 M sorbitol was able to proceed normally by recruiting almost the same number of
229 fimbrin molecules as in walled cells, but with a slightly longer timing (Figure 4F). In
230 contrast, in medium with 1.2 M sorbitol, the timing of fimbrin recruitment was
231 dramatically longer, and endocytosis failed to proceed normally, as reported by the
232 virtually null speed of patches during the entire time fimbrin was present at the
233 endocytic site (Figure 4F). Cells lacking eisosomes showed very similar phenotypes
234 but endocytosis started failing at 0.8 M sorbitol (Figure 4G).

235 At 0.25 M sorbitol, both wild-type and *pil1Δ* protoplasts were able to perform
236 endocytosis but required a larger amount of Fim1p (Figure 4F and 4G). In these
237 conditions, the eisosomes covered only half of the plasma membrane surface area
238 they cover at 0.4M sorbitol (Figure 4B and C) and our data suggest the plasma
239 membrane was under high tension (Figure 4E). This result indicates that during CME
240 the actin machinery is able to adapt to mechanical cues by mechanisms that are
241 independent of the cell wall.

242 For both wild-type and *pil1Δ* protoplasts in 0.4 M sorbitol, the temporal evolution
243 of the number of fimbrin molecules and the speed of patches were close to the same
244 metrics measured in walled cells in media without sorbitol (Figure 4F and 4G). These
245 results suggest that the osmotic pressure at these concentrations, which are

246 equivalent to a pressure of 1 MPa, is close to the naturally maintained turgor
247 pressure of walled fission yeast cells, in good agreement with previous
248 measurements (Minc et al., 2009). Therefore, to keep protoplasts in conditions close
249 to walled cells, the steady state media used in our following experiments on
250 protoplasts contained 0.4 M sorbitol.

251

252 **In protoplasts, eisosomes buffer moderate hypotonic shocks, and the** 253 **endocytic actin machinery rapidly adapts to increases in membrane tension**

254 To characterize the adaptation of the endocytic actin machinery to a rapid
255 increase in turgor pressure and membrane tension, we repeated our acute hypotonic
256 shocks ($\Delta P = -0.05$ M, -0.1 M or -0.2 M) on protoplasts initially at steady state in media
257 containing 0.4 M sorbitol. After low ($\Delta P = -0.05$ M) and medium ($\Delta P = -0.1$ M) acute
258 shocks in wild-type protoplasts, we did not observe any stalled endocytic events –
259 when cells started the recruitment of the actin machinery, endocytosis proceeded to
260 successful completion (Figure 5A, 5B, 5C and Figure 5 Supplement 3). The
261 recruitment of fimbrin did not significantly change over time. In contrast, two minutes
262 after a $\Delta P = -0.2$ M shock, endocytic sites recruited 20% more fimbrin and it took
263 ~25% longer to perform endocytosis (Figure 5C, 5D, and Figure 5 Supplement 3).
264 The actin machinery restored its steady state behavior less than 4 minutes after the
265 shock (Figure 5D).

266 We repeated these experiments with *pil1* Δ protoplasts to eliminate the role of
267 eisosomes in the reduction of membrane tension during hypotonic shocks.
268 Immediately (0 minutes) after the lowest hypotonic shock tested ($\Delta P = -0.05$ M),
269 fimbrin recruitment took slightly longer and the number of proteins recruited was
270 higher than at steady state (Figure 5E, 5F and 5G, Figure 5 Supplement 4). While
271 fimbrin restored its steady-state dynamics in less than 4 minutes after high acute
272 hypotonic shock ($\Delta P = -0.2$ M) in wild-type protoplasts (Figure 5D), recovery of fimbrin
273 dynamics to its steady state behavior in *pil1* Δ protoplasts occurred over 10 minutes,
274 even for the most modest hypotonic shock, $\Delta P = -0.05$ M (Figure 5G). The changes in
275 fimbrin dynamics in *pil1* Δ protoplasts became increasingly larger for $\Delta P = -0.1$ M and
276 $\Delta P = -0.2$ M hypotonic shocks – endocytic sites assembled a peak number of fimbrin
277 respectively ~25% and ~50% larger and took ~85% and ~50% longer. In addition,
278 most cells were unable to survive more than two minutes after these high hypotonic
279 shocks (Figure 6A, 6B, 6C and Figure 6 Supplement 1), which prevented us from
280 determining how the actin machinery recovers after large hypotonic shocks in *pil1* Δ
281 protoplasts.

282 Wild-type protoplasts at steady state in 0.25 M sorbitol contain significantly fewer
283 assembled eisosomes despite expressing normal amounts of Pil1p (Figure 4B and
284 4C). We took advantage of this condition to test whether the absence of eisosomes
285 structures at the plasma membrane and not the absence of the protein Pil1p is
286 responsible for changes in actin dynamics after an acute hypotonic shock. We
287 subjected wild-type protoplasts at steady state in 0.25 M sorbitol to an acute
288 hypotonic shock of $\Delta P = -0.1$ M (Figure 5H and 5I). Two minutes after the shock,
289 endocytic sites accumulated 73% more fimbrin and took ~60% longer (Figure 5H,
290 Figure 5 Supplement 5A). This behavior was nearly identical to fimbrin dynamics in
291 *pil1* Δ protoplasts under the same conditions (Figure 5I, Figure 5 Supplement 5B).
292 Moreover, most wild-type and *pil1* Δ protoplasts were unable to survive longer than 4
293 minutes after these high hypotonic shocks (Figure 5 Supplement 5C). This result
294 further demonstrates that the presence of assembled eisosomes at the plasma

295 membrane is indeed responsible for the adaptation of cells to acute hypotonic
296 shocks, and the presence of Pil1p in the cytoplasm is not sufficient for this response.

297 Altogether, these series of experiments demonstrate that a) eisosomes protect
298 protoplasts from changes in their membrane tension, but only to a small extent, b)
299 without eisosomes, protoplasts can withstand only minor increase in their membrane
300 tension, c) the endocytic actin machinery adapts to compensate the increase in
301 membrane tension, and d) actin dynamics restores its steady state behavior within a
302 few minutes, providing the protoplasts survived the hypotonic shock.

303

304 **Eisosomes protect the integrity of walled cells during consecutive osmotic** 305 **shocks**

306 We observed that a significant number of both wild-type and *pil1Δ* protoplasts
307 died after osmotic shocks, and the percentage of *pil1Δ* protoplasts that remained
308 alive was significantly smaller than for wild-type protoplasts even under moderate
309 shocks ΔP of -0.05 M, -0.1 M and -0.2 M (Fig. 6A-C). In contrast, we found that both
310 wild-type and *pil1Δ* walled cells can survive a single hypotonic shock of $\Delta P=-1.2$ M,
311 which initially led us to think that eisosomes only have a minor protective role in
312 walled cells. However, we noticed that subsequent osmotic shocks lead to higher
313 mortality of *pil1Δ* compare to wild-type walled cells. While almost all the wild-type
314 walled cells remained alive after several shocks, around 10% of *pil1Δ* walled cells
315 died after each subsequent shock (Fig. 6D-F; supplementary video 1 and 2). These
316 results demonstrate that, even in walled cells, eisosomes exert a protective role,
317 likely by buffering sudden changes in membrane tension.

318

319 **Membrane tension and eisosomes modulate the rate of endocytosis in cells**

320 The fast recovery of the actin machinery after an acute change in turgor pressure
321 and membrane tension (Figures 5D and 5G) cannot be explained by the sole release
322 of membrane via eisosome disassembly which happens on a slightly shorter
323 timescale and releases only a small surface area of membrane (Figure 4H and 4I).
324 We hypothesized that a decrease in the number of endocytic events happening in the
325 cell over the same period of time would gradually increase the surface area of the
326 plasma membrane, and therefore reduce membrane tension. We measured the
327 endocytic density, i.e. the number of endocytic events in a cell normalized by the cell
328 length, in wild-type and *pil1Δ* cells after a hypotonic shock using a ratiometric method
329 (Berro and Pollard, 2014a). For all shocks tested in wild-type ($\Delta P=-0.05$ M, -0.1 M, -
330 0.2 M) and *pil1Δ* protoplasts ($\Delta P=-0.025$ M, -0.05 M, -0.1 M) initially at steady state in
331 0.4 M sorbitol, the endocytic density in protoplasts significantly decreased
332 immediately after the hypotonic shock (Figure 7A). The difference increased for
333 increasing hypotonic shocks, up to 36% for wild-type protoplasts after a $\Delta P=-0.2$ M
334 shock, and 79% for *pil1Δ* protoplasts after a $\Delta P=-0.1$ M shock (Figure 7B). These
335 abrupt changes in the endocytic density were followed by a 2- to 6-minute recovery
336 back to the steady-state endocytic density, and recovery time depended on the
337 magnitude of the hypotonic shock. The temporal variations of the endocytic density
338 after hypotonic shocks mirrored the changes in Fim1p dynamics in endocytic patches
339 in similar conditions (Figure 5C, 5D, 5F and 5G). Note that the change in cell volume
340 (Figure 7A & 7B, insets) could not exclusively account for the observed decrease in
341 the endocytic density as the volume increased faster than the change in endocytic
342 density.

343 Building on these results in protoplasts, we wondered whether the endocytic
344 density in walled cells also adapts to hypotonic shocks. Indeed, immediately after the

345 largest shock tested ($\Delta P = -1.2$ M), we observed a similar decrease in the endocytic
346 density for both wild-type and *pil1 Δ* walled cells, 36% and 46% respectively (Figure
347 7C). Recovery to steady-state endocytic densities occurred in less than 2 minutes in
348 both wild-type and *pil1 Δ* walled cells, faster than in protoplasts (Figure 7A, 7B and
349 7C). These results were surprising because we detected virtually no difference in the
350 dynamics of fimbrin recruitment to endocytic sites in both strains (Figure 2E). Our
351 data show that the cell wall limits but does not completely cancel the effect of
352 hypotonic shocks. They also suggest that the regulation of the endocytic density
353 supplements the regulation performed by the eisosomes to reduce membrane
354 tension and enable normal actin machinery dynamics at endocytic sites.

355 Wild-type and *pil1 Δ* walled cells had a very similar adaptation after hypotonic
356 shocks. However, we noticed a difference in the endocytic density at steady state in
357 different sorbitol concentrations. For all concentrations tested (0 to 2 M), wild-type
358 cells maintained roughly the same endocytic density. In contrast, the steady state
359 endocytic density in *pil1 Δ* cells increased with increasing media osmolarity, up to
360 56% in 2 M sorbitol (Figure 7D). Our results suggest that eisosomes participate in
361 maintaining a constant density of endocytosis independently of the media osmolarity,
362 not only after an abrupt change in membrane tension, but also when they are at
363 steady state in different osmolarity.

364

365 **The exocytosis rate increases after a hypotonic shock in protoplasts but not in** 366 **walled cells**

367 Reciprocal to the decrease in the number of endocytic events observed after a
368 hypotonic shock, we wondered whether the rate of exocytosis increases in the
369 meantime to provide more surface area to the plasma membrane, as it has been
370 observed in mammalian cells (Gauthier et al., 2009).

371 To measure the rate of exocytosis in different conditions, we used the cell
372 impermeable styryl dye FM4-64, whose fluorescence dramatically increases when it
373 binds to membranes, to measure the increase of cell surface area due to vesicle
374 fusion (Cochilla et al., 1999; Gachet and Hyams, 2005; Richards et al., 2000). After
375 FM4-64 is introduced to the media, fusion of unstained intracellular vesicles to the
376 plasma membrane results in an increase of total cell fluorescence, because after
377 each fusion event new unstained membrane is exposed to the dye. Note that
378 endocytic events do not increase the total cell fluorescence because they transfer
379 already stained patches of the plasma membrane into the interior of the cell (Figure
380 8A). Note also that the increase in total cell fluorescence could also be due to
381 putative transfer of lipids by non-exocytic mechanisms but for simplicity and by lack
382 of further evidence, onwards we will interpret the increase in fluorescence to an
383 increase in the exocytosis rate.

384 Staining of wild-type fission yeast with 20 μ M FM4-64 in EMM5S (Figure 8B)
385 showed that after a brief phase of rapid staining of the cell surface, the total cell
386 fluorescence intensity grows linearly for at least 20 minutes, and the slope of the
387 normalized intensity corresponds to the exocytosis rate as a percentage of the
388 plasma membrane surface area per unit of time (see materials and methods)
389 (Gauthier et al., 2009; Smith and Betz, 1996; Vida and Emr, 1995). Using this
390 method, we measured that wild-type walled cells at steady state in EMM5S
391 exocytose 4.6% of their plasma membrane surface area per minute (Figure 8B).
392 FM4-64 staining did not seem to affect the endocytic and exocytic membrane
393 trafficking of yeast cells, since stained vesicles are successfully released after
394 washing cells with fresh media (Figure 8B).

395 We measured the exocytosis rates in the conditions that had the largest
396 effects on endocytosis while keeping most cells alive, i.e. we used protoplasts at
397 steady state in 0.4 M and performing a $\Delta P = -0.2$ M shock for wild-type and $\Delta P = -0.05$
398 M shock for *pil1* Δ . At steady state in 0.4M sorbitol (Figure 8C and 8E), wild-type
399 protoplasts had an exocytosis rate similar to walled cells in EMM5S in 0 M ($k_{0-5} = 4.4 \pm 0.2\% \text{ min}^{-1}$). After a $\Delta P = -0.2$ M shock, the exocytosis rate increased by 41%
400 ($k_{0-5} = 6.2 \pm 0.4\% \text{ min}^{-1}$). At steady state in 0.4 M sorbitol (Figure 8D and 8E), the
401 exocytosis rate of *pil1* Δ protoplasts was higher than for walled cells in 0 M sorbitol
402 ($k_{0-5} = 6.2 \pm 0.4\% \text{ min}^{-1}$). After a $\Delta P = -0.05$ M shock, the exocytosis rate increased
403 modestly ($k_{0-5} = 6.8 \pm 0.5\% \text{ min}^{-1}$). Therefore, in both wild-type and *pil1* Δ protoplasts, an
404 acute hypotonic shock leads to an increased exocytosis rate, which increases
405 surface area and likely reduces membrane tension. The change in exocytosis rate in
406 *pil1* Δ protoplasts being more modest than in wild-type cells highlights the role of
407 eisosomes in buffering the change in the exocytosis rate in response to change in
408 osmolarity and membrane tension.
409

410 We wondered whether these changes in exocytosis rate also happen in walled
411 cells. First, we measured exocytosis rate at steady state in solutions with different
412 molarities and found that the rates were smaller than in protoplasts (Figures 8F, 8G,
413 and 8H). The exocytosis rate of wild-type walled cells at steady state in 1.2M sorbitol
414 ($k_{0-5} = 3.1 \pm 0.1\% \text{ min}^{-1}$, Figure 8F and 8H) was 35% smaller than in 0 M sorbitol ($k_{0-5} = 4.8 \pm 0.1\% \text{ min}^{-1}$, Figure 8B). In addition, in *pil1* Δ walled cells, the exocytosis rate of
415 walled cells lacking eisosomes in 1.2M sorbitol was only slightly smaller than wild-
416 type cells in the same conditions ($k_{0-5} = 2.6 \pm 0.1\% \text{ min}^{-1}$, Figure 8G and 8H). After
417 hypotonic shocks, the change of exocytosis rate in walled cells was very limited
418 (Figure 8F-H). In fact, our strongest hypotonic shock of $\Delta P = -1.2$ M did not
419 significantly increase the exocytosis rate of wild-type or *pil1* Δ cells walled cells
420 (Figure 8H). These data corroborate our previous finding that the cell wall limits but
421 does not completely cancel the effect of hypotonic shocks in intact cells. In addition,
422 they also demonstrate that eisosomes are involved in the regulation of the exocytosis
423 rate.
424

425 **Inhibition of exocytosis decreased the survival rate of protoplasts under acute** 426 **hypotonic shock.** 427

428 To further test our hypothesis that reducing the endocytosis rate and
429 increasing the exocytosis rate help regulate membrane tension after a hypotonic
430 shock, we wondered whether blocking endocytosis or exocytosis with drugs would
431 affect the survival rates of cells. We hypothesized that inhibition of endocytosis or
432 exocytosis would have opposite effects on the survival of protoplasts under acute
433 hypotonic shock. Specifically, inhibition of endocytosis would help retain membrane
434 on the surface of protoplasts, thereby reducing the probability of membrane rupture,
435 and, conversely, inhibition of exocytosis would reduce the transfer of membrane from
436 intracellular vesicles to the surface of protoplasts, exasperating the lack of plasma
437 membrane in the face of imminent protoplast expansion. To observe the largest
438 effects, we used *pil1* Δ protoplasts under $\Delta P = -0.2$ M shock, and exposed the cells to
439 either Latrunculin A (LatA) or Brefeldin A (BFA) for 30 minutes before the shocks.

440 Blocking exocytosis with BFA increases the death rate of protoplasts after
441 hypotonic shocks, confirming our hypothesis (Figure 9 and Figure 9 Supplement 1).
442 Blocking actin assembly, and therefore endocytosis, with LatA made the protoplasts
443 more resistant starting 4 minutes after the hypotonic shock, also confirming our

444 hypothesis. Note that LatA treatment made the protoplasts less resistant to shock in
445 the initial 2 minutes after the hypotonic shock, which seems in contradiction with our
446 hypothesis. However, it is possible that prolonged treatment with LatA had other
447 unidentified effects on protoplasts survival or may indirectly affect the exocytosis rate
448 since LatA affects all actin structures in the cell, including actin cables which are
449 needed for the transport of exocytic vesicles (Lo Presti et al., 2012).

450

451 Discussion

452 **Robustness of CME in fission yeast**

453 Our data demonstrate that CME is able to proceed in a wide range of
454 osmolarities and membrane tension. Even cells devoid of a cell wall and eisosomes
455 were able to perform endocytosis after an acute change in membrane tension, as
456 long as their plasma membrane was not damaged and cells remained alive. Even in
457 the most extreme conditions tested, i.e. cells devoid of a cell wall and lacking the
458 majority of their eisosomes, the dynamics of fimbrin at endocytic sites was only two
459 times larger than what was observed in wild-type walled cells. These results
460 demonstrate that not only are cells able to adapt their endocytic machinery to acute
461 changes in membrane tension but, they are also able to rapidly regulate their
462 membrane tension.

463

464 **Mechanisms of tension regulation and homeostasis of the plasma membrane**

465 Our results demonstrate that the regulation of membrane tension in hypotonic
466 environment is performed via a combination of at least three mechanisms: the
467 mechanical protection by the cell wall, the disassembly of the eisosomes and the
468 temporary shift in the balance between endocytosis and exocytosis (Figure 10). Our
469 data indicate that all three mechanisms are used in parallel, since wild-type walled
470 cells are less sensitive to acute hypotonic shocks than wild-type protoplasts and
471 *pil1Δ* walled cells, and they experience a temporary decrease in their endocytic
472 density for about 2 minutes after the shock. In addition, our data allow us to estimate
473 the relative contribution of each mechanism in the regulation of membrane tension.

474 The cell wall provides the largest protection during chronic and acute changes
475 in media osmolarity. Wild-type walled cells are virtually insensitive to osmotic
476 changes, and *pil1Δ* walled cells are much less sensitive than *pil1Δ* protoplasts.
477 Removal of the cell wall dramatically affects actin dynamics at endocytic sites and
478 eisosome assembly at the plasma membrane (Figure 4B, 4C, 4F and 4G), and
479 greatly increased the effect of hypotonic shock on exocytosis (Figure 8C-F). It is
480 surprising that endocytosis in protoplasts still proceeds in media with osmolarity as
481 low as 0.25 M, where a large fraction of eisosomes is disassembled. In fact, the actin
482 endocytic machinery can overcome membrane tensions high enough to rupture the
483 plasma membrane since we did not see stalled actin patches, or actin comet tails, in
484 any of our experiments. Our results contrast with recent data in *S. cerevisiae* (Riggi
485 et al., 2019) where endocytosis is blocked and actin comet tails are formed within 2
486 minutes of a hypotonic shock. These differences may highlight species specificities.

487 Our results add to a growing body of evidence that eisosomes play a critical
488 role in the regulation of membrane tension and membrane integrity through dynamic
489 remodeling and scaffolding of the plasma membrane (Kabeche et al., 2015; Moseley,
490 2018). Endocytosis in wild-type walled cells are not sensitive to chronic or acute
491 hypotonic changes, whereas *pil1Δ* walled cells are (Figure 2 and Figure 3).

492 Conversely, exocytosis seems to respond more strongly to acute hypotonic shock in
493 wild-type walled cells than in *pil1Δ* walled cells (Figure 8E and 8F). The protective
494 role of eisosomes is even more striking in protoplasts under acute hypotonic shocks.
495 Wild-type protoplasts whose plasma membrane is covered with eisosomes are
496 largely insensitive to increases in membrane tension whereas protoplasts with little to
497 no eisosomes are extremely sensitive to increases in membrane tension and their
498 plasma membrane is easily damaged (Figure 6A-C). Eisosomes retain this protective
499 function even in walled cells, which becomes evident when cells are put under
500 repeated osmolarity shocks (Figure 6D-F). Our micropipette aspiration experiments
501 also demonstrate that eisosomes are critical to keep membrane tension low during
502 an acute hypotonic shock. Therefore, our data indicate that membrane tension is
503 decreased via the disassembly of eisosomes, through release of excess membrane
504 surface area. Assuming eisosomes are hemi-cylinders with diameter ~50 nm and
505 cells contain 1.6 μm of eisosomes per μm^2 of plasma membrane on average, total
506 eisosome disassembly could release about 5% of the total surface area of the
507 plasma membrane over ~3 minutes after a hypotonic shock (Kabeche et al., 2015),
508 although a mild shock of $\Delta P = -0.2$ M disassembled close to ~50% eisosomes over 5
509 minutes, or about 2.5% of the surface area of the plasma membrane (Figure 4H and
510 4I). Recent single-molecule imaging in our lab demonstrated that at steady state
511 Pil1p undergoes rapid exchange at the eisosome ends (Lacy et al., 2017), potentially
512 providing a convenient route for rapid disassembly of the BAR domain-mediated
513 scaffold, analogous to filament depolymerization, in combination with eisosome
514 breaking. Disassembled eisosome components have altered phosphorylation level or
515 sub-cellular localization, which potentially relays the signaling from eisosome integrity
516 to endocytosis and/or exocytosis (Riggi et al., 2018; Walther et al., 2007), possibly
517 via TORC2 (Riggi et al., 2019).

518 Our study highlights a third mechanism to reduce membrane tension by
519 increasing the surface area of the plasma membrane via a temporary reduction in the
520 endocytosis rate and an increase in the exocytosis rate. Using our data, we estimate
521 that cells endocytose about 2% of their surface area per minute through clathrin
522 mediated endocytosis, confirming our previous measurements (Berro and Pollard,
523 2014a, 2014b). During acute hypotonic shock, a reduction of the endocytosis rate
524 plus an increase in the exocytosis rate for a few minutes would allow for a net
525 addition of surface area to the plasma membrane. For example, in *pil1Δ* protoplasts
526 initially at steady state in 0.4 M sorbitol the endocytosis rate is reduced by ~25 % for
527 ~10 minutes after an acute hypotonic shock of $\Delta P = -0.05$ M, while the exocytosis rate
528 increased by ~10%. The net surface area added over that period by reduction in
529 endocytosis and increase in exocytosis corresponds to a 5% + 6% = 11% increase in
530 the protoplast surface area, close to the ~12% surface area increase we measured.
531 These results confirm and quantify previous reports of control of surface tension by
532 increasing the surface area via a modulation of endocytosis and exocytosis rates in
533 other eukaryotes (Apodaca, 2002; Homann, 1998; Morris and Homann, 2001). These
534 estimates demonstrate that modulating the endocytosis and exocytosis rates is an
535 efficient way to increase the surface area of the plasma membrane by large amounts,
536 but this process is relatively slow compared to eisosome disassembly. The slowness
537 of this process might explain why *pil1Δ* and pre-stretched wild-type protoplasts that
538 have about half the normal amount of eisosomes on their surface do not survive even
539 relatively small hypotonic shocks, being unable to provide enough membrane in a
540 short amount of time to reduce the tension of their plasma membrane.

541

542 **Molecular mechanisms driving the adaptation of the actin endocytic machinery**
543 **and the rate of endocytosis under various membrane tensions**

544 Under conditions where membrane tension and turgor pressure were
545 significantly increased, we observed that the endocytic actin machinery took longer
546 and assembled a larger number of fimbrin molecules to successfully produce
547 endocytic vesicles. This effect increased with increasing membrane tension, up to
548 tensions high enough to rupture the cell plasma membrane. This result strongly
549 supports the idea that the actin machinery provides the force that counteracts
550 membrane tension and turgor pressure and deforms the plasma membrane into an
551 endocytic pit.

552 The precise molecular mechanism that regulates this enhanced assembly
553 remains to be uncovered. Our data suggest that actin dynamics is controlled via a
554 mechanical or geometrical regulation, where actin assembles until the plasma
555 membrane is deformed and pinched off. An alternative, and non-mutually exclusive,
556 hypothesis is that the activity and/or recruitment of proteins upstream of the actin
557 nucleators may be enhanced by increased membrane tension. A third hypothesis is
558 that the decrease in the number of endocytic events after an increase in membrane
559 tension leads to an increase in the concentration of endocytic proteins in the
560 cytoplasm, which can then enhance the reactions performed at the endocytic sites.
561 Sirotkin et al (Sirotkin et al., 2010) measured that 65% to 85% of the total cellular
562 content of key proteins involved in the endocytic actin machinery are localized to
563 endocytic sites at any time. A 20% decrease in the number of endocytic sites would
564 increase their cytoplasmic abundance by roughly 40% to 80%. This percentage is
565 larger than the volume changes we measured, resulting in a net increase in the
566 cytoplasmic concentration of these proteins, which would allow larger amount of
567 protein to assemble at the endocytic sites.

568 Conversely, the decreased endocytosis rate could be attributed to the larger
569 number of endocytic proteins assembled at each endocytic sites, which would
570 decrease their cytoplasmic concentration. Indeed, Burke *et al.* (Burke et al., 2014)
571 showed that modulating actin concentration modulates the number of endocytic sites
572 in the same direction. However, it is more likely that one or several early endocytic
573 proteins are sensitive to membrane tension, and either fail to bind the plasma
574 membrane or prevent the triggering of actin assembly when membrane tension is
575 high. This idea would be consistent with results from mammalian cells demonstrating
576 that the proportion of stalled clathrin-coated pits increases when membrane tension
577 increases (Ferguson et al., 2017). In addition, several endocytic proteins that arrive
578 before or concomitantly with the activators of the actin machinery contain BAR
579 domains (such as Syp1p, Bzz1p and Cdc15p), and other members of this domain
580 family (which also includes Pil1p) have been shown to bind membranes in a tension-
581 sensitive manner. Further quantitative study of early endocytic proteins will help
582 uncover the validity and relative contributions of each one of these hypotheses.

583 We expect our results to be relevant to the study of CME and membrane
584 tension regulation in higher order eukaryotes. Indeed, the molecular machineries for
585 endocytosis, exocytosis and osmotic response are highly conserved between fission
586 yeast and other eukaryotes. In addition, regulation of membrane tension and CME
587 are particularly critical during cell polarization (Mostov et al., 2000), during neuron
588 development and shape changes (Urbina et al., 2018) and at synapses where large
589 pools of membranes are added and retrieved on a very fast time scale (Nicholson-
590 Fish et al., 2016; Watanabe and Boucrot, 2017).

591

592 **Materials and Methods**

593 **Yeast strains and media**

594 The *S. pombe* strains used in this study are listed in Supplemental Table S1.
595 Yeast cells were grown in YE5S (Yeast Extract supplemented with 0.225 g/L of
596 uracil, lysine, histidine, adenine and leucine), which was supplemented with 0 to 1.2
597 M D-Sorbitol, at 32°C in exponential phase for about 18 hours. Cells were washed
598 twice and resuspended in filtered EMM5S (Edinburgh Minimum media supplemented
599 with 0.225 g/L of uracil, lysine, histidine, adenine and leucine), which was
600 supplemented with the same concentration of D-Sorbitol, at least 10 minutes before
601 imaging so they can adapt and reach steady state.

602

603 **Protoplasts preparation**

604 *S. pombe* cells were grown in YE5S at 32°C in exponential phase for about 18
605 hours. 10 mL of cells were harvested and washed two times with SCS buffer (20 mM
606 citrate buffer, 1 M D-Sorbitol, pH=5.8), and resuspended in SCS supplemented with
607 0.1 g/mL Lallzyme (Lallemand, Montreal, Canada) (Flor-Parra et al., 2014). Cells
608 were incubated with gentle shaking for 10 minutes at 37°C in the dark except for
609 experiments in Figure 9, where cells were digested at room temperature with gentle
610 shaking for 30 minutes in the presence of inhibitors. The resulting protoplasts were
611 gently washed twice in EMM5S with 0.25 to 1.2 M D-Sorbitol, spun down for 3
612 minutes at 0.4 rcf between washes, and resuspended in EMM5S buffer
613 supplemented with 0.25 to 1.2 M D-Sorbitol at least 10 minutes before imaging so
614 they can adapt and reach steady state.

615

616 **Microscopy**

617 Microscopy was performed using a spinning disk confocal microscope, built on
618 a TiE inverted microscope (Nikon, Tokyo, Japan), equipped with a CSU-W1 spinning
619 head (Yokogawa Electric Corporation, Tokyo, Japan), a 100X/1.45NA Phase
620 objective, an iXon Ultra888 EMCCD camera (Andor, Belfast, UK), and the NIS-
621 Elements software v. 4.30.02 (Nikon, Tokyo, Japan) on. The full system was
622 switched on at least 45 minutes prior to any experiments to stabilize the laser power
623 and the room temperature. Cells were loaded into commercially available
624 microfluidics chambers for haploid yeast cells (Y04C-02-5PK, Millipore-Sigma, Saint-
625 Louis, USA) for the CellASIC ONIX2 microfluidics system (Millipore-Sigma, Saint-
626 Louis, USA). Each field of view was imaged for 60 seconds, and each second a stack
627 of 6 z-slices separated by 0.5 μm was imaged. The microscope was focused such
628 that the part of the cell closest to the coverslip was captured.

629

630 **Acute hypotonic shocks**

631 Walled cells or protoplasts were first imaged in their steady state media
632 (EMM5S supplemented with 0 to 1.2 M D-Sorbitol). The steady state media was
633 exchanged with media supplemented with a lower D-Sorbitol concentration (the
634 concentration difference is noted ΔP), with inlet pressure of 5 psi. This hypotonic
635 shock media was labelled with 6.7 $\mu\text{g}/\text{mL}$ of sulforhodamine B (MP Biomedicals LLC,
636 Santa Ana, USA), a red cell-impermeable dye that allowed us to a) monitor the full
637 exchange of the solution in the microfluidic chamber prior to image acquisition, and
638 b) monitor the plasma membrane integrity of the cells after the shock. In each
639 condition, the first movie was started when the sulforhodamine B dye was visible in

640 the field of view. For clarity, this time point is labelled $t=0$ min in all our figures, but
641 note that we estimate it may vary by up to ~ 30 seconds between movies and
642 conditions. We imaged cells by taking one stack of 6 Z-slices per second for 60
643 seconds. After the end of each movie, we rapidly changed field of view and restarted
644 acquisition one minute after the end of the previous movie, so that movies started
645 every 2 minutes after the acute hypotonic shock. Tracks from cells that contained red
646 fluorescence from the sulforhodamine B dye were excluded from the analysis,
647 because this indicated that cell membrane had been damaged.

648 **Inhibition of endocytosis and exocytosis during acute hypotonic shock**

649 Endocytosis or exocytosis was inhibited by including respectively 25 μ M
650 Latrunculin A (Millipore, MA, USA) or 2mM Brefeldin A (Santa Cruz Biotechnology
651 Inc., TX, USA) in the solution used to prepare the protoplasts and and to perform the
652 hypotonic shocks. Hypotonic shock solution also included 20 μ M FM4-64 (Biotium,
653 Fremont, CA, USA) to stain dead protoplasts (Vida and Gerhardt, 1999) (Figure 9
654 Supplement 1), and inlet pressure was set at 4 psi.

655 **Measurement of the temporal evolution of the number of proteins and speed**

656 Movies were processed and analyzed using an updated version of the
657 PatchTrackingTools toolset for the Fiji (Schindelin et al., 2012) distribution of ImageJ
658 (Berro and Pollard, 2014a; Schneider et al., 2012). This new version includes
659 automatic patch tracking capabilities based on the Trackmate library (Tinevez et al.,
660 2017), and is available on the Berro lab website:
661 [http://campuspress.yale.edu/berrolab/
662 publications/software/](http://campuspress.yale.edu/berrolab/publications/software/). Prior to any quantitative measurements, we corrected our
663 movies for uneven illumination and camera noise. The uneven illumination was
664 measured by imaging a solution of Alexa 488 dye and the camera noise was
665 measured by imaging a field of view with 0% laser power. We tracked Fim1-mEGFP
666 spots with a circular 7-pixel diameter region of interest (ROI), and measured the
667 temporal evolution of the fluorescence intensities and the position of the centers of
668 mass. The spot intensity was corrected for cytoplasmic background using a 9-pixel
669 median filter, and was then corrected for photobleaching. The photobleaching rate
670 was estimated by fitting a single exponential to the temporal evolution of the intensity
671 of cytoplasmic ROIs void of any identifiable spots of fluorescence (Berro and Pollard,
672 2014a). Only tracks longer than 5 s and displaying an increase followed by a
673 decrease in intensity were kept for the analysis. Individual tracks were aligned and
674 averaged with the temporal super-resolution algorithm from (Berro and Pollard,
675 2014a), and post-processed using custom scripts in Matlab R2016a (Mathworks). In
676 brief, this method realigns temporal signals that have low temporal resolution and
677 where no absolute time reference is available to align them relatively to each other. It
678 iteratively finds the temporal offset which has a higher precision than the measured
679 signal and minimizes the mean square difference between each measured signal
680 and a reference signal. For the first round of alignments, the reference signal is one
681 of the measurements. After each realignment round, a new reference is calculated as
682 the mean of all the realigned signals, which is an estimator of the true underlying
683 signal.

684 To control and calibrate the intensity of our measurements, we imaged wild-
685 type walled cell expressing Fim1p-mEGP each imaging day. Intensities were
686 converted into number of molecules with a calibration factor such that the peak
687 intensity of our control strain corresponded to 830 molecules (Berro and Pollard,
688
689

690 2014a).

691 In all figures presenting the temporal evolution of the number of molecules or
692 the speed, time 0 s corresponds to the time point when the number of molecules is
693 maximum (also called the peak number). Statistical tests between conditions were
694 performed at time 0 s with a one-way ANOVA test using the number of tracks
695 collected to build the figure. To avoid extrapolating the data, we compared the
696 relative duration of assembly and disassembly between conditions using the time at
697 which the average number of molecules reach half the peak number.

698 **Measurement of the density of CME events**

699 We used the *S. Pombe* profiling tools for ImageJ (Berro and Pollard, 2014a) to
700 measure the number of endocytic events at a given time in each cell. In brief, on a
701 sum-projected z-stack, we manually outlined individual cells, and, for each position
702 along the long axis of a cell, we measured the sum of fluorescence orthogonal to the
703 long axis. We corrected the intensity profile in each cell for its cytoplasmic intensity
704 and media fluorescence outside the cell. We estimated the number of patches in
705 each cell by dividing the corrected fluorescence signal with the temporal average of
706 the fluorescence intensity of one endocytic event. We calculated the linear density of
707 endocytic events as the ratio between the number of endocytic events in a cell and
708 its length.

709 **Measurement of the exocytosis rate with FM4-64 staining**

710 The exocytosis rate was measured by combining the acute hypotonic shock
711 with FM4-64 staining, in a similar approach as has been reported (Gauthier et al.,
712 2009; Smith and Betz, 1996; Vida and Emr, 1995). The cell impermeable dye FM4-
713 64 (Biotium, Fremont, CA, USA) was diluted to a final concentration of 20 μ M in any
714 of the media used. When cells are exposed to FM4-64, the dye rapidly stains the
715 outer leaflet of the plasma membrane. Upon endocytosis, the dye is trafficked inside
716 the cell without change in fluorescence. The total cell fluorescence intensity was
717 measured after segmenting the cells by thresholding the fluorescence signal above
718 background levels. The fluorescence intensity was normalized to the intensity
719 reached at the end of the fast increase \sim 1 min after the dye was flowed in, which
720 corresponds to the intensity of total surface area of the plasma membrane (Figure
721 8B). After this fast phase ($<$ 20 seconds), the fluorescence signal increased more
722 slowly every time unstained membrane was exposed to the cell surface by
723 exocytosis. At short time scale (\sim 5 to 20 min depending on the exocytosis rate),
724 recycling of stained membrane is negligible and one can assume that all exocytosed
725 membrane is virtually unstained. Since the intensity at the beginning of the slow
726 phase was normalized to 1, the slope of the linear increase of fluorescence is equal
727 to the amount of membrane exocytosed per minute, expressed as a fraction of the
728 surface area of the plasma membrane. For all measurements, images were taken at
729 5 s interval at the midline of cells with the help of Perfect Focusing System (Nikon,
730 Tokyo, Japan), with minimal laser excitation in order to reduce toxicity and
731 photobleaching to negligible values. Curve fitting and slope calculation was
732 performed in GraphPad Prism (GraphPad Software, La Jolla, CA, USA).

733

734 **Measurement of eisosomes' density on the plasma membrane**

735 We imaged full cells expressing Pil1p-mEGFP by taking stacks of 0.5 μ m
736 spaced Z-slices. We corrected these Z-stacks for uneven illumination and manually
737 outlined individual cells to determine the surface area of each cell. To determine the

738 total amount of eisosome-bound Pil1p-mEGFP we subtracted the cytosolic intensity
739 of Pil1-mEGFP using a pre-determined threshold and summed all the Z-slices. We
740 measured the mean membrane intensity of each cell on the thresholded sum-
741 projection image. The eisosome density was determined by dividing this mean
742 intensity by the surface area of each protoplast.

743 To quantify the relative changes in area fraction of eisosomes after acute
744 hypotonic shock, wild-type protoplasts expressing Pil1p-mEGFP were loaded into
745 ONIX2 microfluidics system (Millipore-Sigma, Saint-Louis, USA), and time lapse
746 fluorescent images were taken at a single Z-slice at the top of protoplasts during
747 media change. After background correction, the total area fraction of eisosomes at
748 the beginning of hypotonic shock was set to 1.0 for normalization, and the normalized
749 values of area fraction were fit to a single exponential decay curve in GraphPad
750 Prism (GraphPad Software, La Jolla, CA, USA).
751

752 **Measurement of membrane tension**

753 Protoplasts were loaded in a custom-built chamber which was passivated with
754 0.2 mg/mL β -casein (Millipore-Sigma, Saint-Louis, USA) for 30 minutes and pre-
755 equilibrated with EMM5S supplemented with 0.8 M D-Sorbitol. A glass micropipette
756 (#1B100-4, World Precision Instruments, Sarasota, USA) was forged to a diameter
757 smaller than the average protoplast radius ($\sim 2.5 \mu\text{m}$), and was connected to a water
758 reservoir of adjustable height to apply a defined aspiration pressure. Before and after
759 each experiment the height of the water reservoir was adjusted to set the aspiration
760 pressure to 0. Cells were imaged with a bright field IX-71 inverted microscope
761 (Olympus, Tokyo, Japan) equipped with a 60X/1.4NA objective, and images were
762 recorded every second. Aspiration pressure was gradually increased every 30 s and
763 the membrane tension σ was calculated as $\sigma = \Delta P \cdot R_p / [2(1 - R_p/R_c)]$, where R_p and
764 R_c are respectively the micropipette and the cell radius, ΔP is the aspiration pressure
765 for which the length of the tongue l of the protoplast in the micropipette is equal to R_p
766 (Evans and Yeung, 1989). To limit the effects of the adaptation of cells' membrane
767 tension, all measurements were performed within the first five minutes after the
768 hypotonic shock, which greatly limited the throughput of our assay (1 measurement
769 per sample), compared to the measurements at steady state (around 6
770 measurements per sample).
771
772

773 **Acknowledgements**

774 We thank Yale West Campus Imaging core for providing access to the spinning disc
775 confocal microscope, members of the Berro lab for insightful discussions and R.
776 Fernandez for providing mutant yeast strains. We thank Ramesh Ramji and Kathryn
777 Miller-Jensen for initial help with the microfluidics part of this project. We gratefully
778 thank Millipore Sigma for lending us a CellASIC unit and Erdem Karatekin for access
779 to his micropipette aspiration setup. We also thank Samantha Dundon, Mike Lacy
780 and Matt Akamatsu for their comments on our manuscript. This research was
781 supported in part by National Institutes of Health/National Institute of General Medical
782 Sciences Grant R01GM115636 and by seed funding from the American Cancer
783 Society Institutional Research Grant #IRG 58-012-58.

785 References

- 786 Aghamohammadzadeh S, Ayscough KR. 2009. Differential requirements for actin
787 during yeast and mammalian endocytosis. *Nature cell biology* **11**:1039–1042.
788 doi:10.1038/ncb1918
- 789 Aghamohammadzadeh S, Smaczynska-de Rooij II, Ayscough KR. 2014. An Abp1-
790 dependent route of endocytosis functions when the classical endocytic
791 pathway in yeast is inhibited. *PLoS ONE* **9**. doi:10.1371/journal.pone.0103311
- 792 Apodaca G. 2002. Modulation of membrane traffic by mechanical stimuli. *American*
793 *Journal of Physiology-Renal Physiology* **282**:F179–F190.
794 doi:10.1152/ajprenal.2002.282.2.F179
- 795 Arasada R, Pollard TD. 2011. Distinct Roles for F-BAR Proteins Cdc15p and Bzz1p
796 in Actin Polymerization at Sites of Endocytosis in Fission Yeast. *Current*
797 *Biology* **21**:1450–1459. doi:10.1016/j.cub.2011.07.046
- 798 Arasada R, Sayyad WAWA, Berro J, Pollard TDTD. 2018. High-speed
799 superresolution imaging of the proteins in fission yeast clathrin-mediated
800 endocytic actin patches. *Molecular Biology of the Cell* **29**:295–303.
801 doi:10.1091/mbc.E17-06-0415
- 802 Atilgan E, Magidson V, Khodjakov A, Chang F. 2015. Morphogenesis of the Fission
803 Yeast Cell through Cell Wall Expansion. *Current biology* □: **CB 25**:2150–7.
804 doi:10.1016/j.cub.2015.06.059
- 805 Basu R, Munteanu EL, Chang F. 2013. Role of turgor pressure in endocytosis in
806 fission yeast. *Molecular biology of the cell* **25**:679–87. doi:10.1091/mbc.E13-
807 10-0618
- 808 Berro J, Lacy MM. 2018. Quantitative Biology of Endocytosis, Colloquium Series on
809 Quantitative Cell Biology (Marshall WF, ed). San Rafael (CA): Morgan &
810 Claypool.
- 811 Berro J, Pollard TD. 2014a. Local and global analysis of endocytic patch dynamics in
812 fission yeast using a new “temporal superresolution” realignment method.
813 *MBoC* **25**:3501–3514. doi:10.1091/mbc.e13-01-0004
- 814 Berro J, Pollard TD. 2014b. Synergies between Aip1p and capping protein subunits
815 (Acp1p and Acp2p) in clathrin-mediated endocytosis and cell polarization in
816 fission yeast. *MBoC* **25**:3515–3527. doi:10.1091/mbc.e13-01-0005
- 817 Berro J, Sirotkin V, Pollard TD. 2010. Mathematical Modeling of Endocytic Actin
818 Patch Kinetics in Fission Yeast: Disassembly Requires Release of Actin
819 Filament Fragments. *MBoC* **21**:2905–2915. doi:10.1091/mbc.e10-06-0494
- 820 Boulant S, Kural C, Zeeh J-C, Ubelmann F, Kirchhausen T. 2011. Actin dynamics
821 counteract membrane tension during clathrin-mediated endocytosis. *Nature*
822 *cell biology* **13**:1124–1131. doi:10.1038/ncb2307
- 823 Burke TA, Christensen JR, Barone E, Suarez C, Sirotkin V, Kovar DR. 2014.
824 Homeostatic actin cytoskeleton networks are regulated by assembly factor
825 competition for monomers. *Current Biology* **24**:579–585.
826 doi:10.1016/j.cub.2014.01.072
- 827 Carlsson AE, Bayly P V. 2014. Force generation by endocytic actin patches in
828 budding yeast. *Biophysical Journal* **106**:1596–1606.
829 doi:10.1016/j.bpj.2014.02.035
- 830 Chen Q, Pollard TD. 2013. Actin Filament Severing by Cofilin Dismantles Actin
831 Patches and Produces Mother Filaments for New Patches. *Current Biology*
832 **23**:1154–1162. doi:10.1016/J.CUB.2013.05.005

- 833 Cheng JPX, Mendoza-Topaz C, Howard G, Chadwick J, Shvets E, Cowburn AS,
834 Dunmore BJ, Crosby A, Morrell NW, Nichols BJ. 2015. Caveolae protect
835 endothelial cells from membrane rupture during increased cardiac output. *The*
836 *Journal of Cell Biology* **211**:53–61. doi:10.1083/jcb.201504042
- 837 Cochilla AJ, Angleson JK, Betz WJ. 1999. MONITORING SECRETORY
838 MEMBRANE WITH FM1-43 FLUORESCENCE. *Annual Review of*
839 *Neuroscience* **22**:1–10. doi:10.1146/annurev.neuro.22.1.1
- 840 Courtemanche N, Pollard TD, Chen Q. 2016. Avoiding artefacts when counting
841 polymerized actin in live cells with LifeAct fused to fluorescent proteins. *Nature*
842 *Cell Biology* **18**:676–683. doi:10.1038/ncb3351
- 843 Davì V, Tanimoto H, Ershov D, Haupt A, De Belly H, Le Borgne R, Couturier E,
844 Boudaoud A, Minc N. 2018. Mechanosensation Dynamically Coordinates
845 Polar Growth and Cell Wall Assembly to Promote Cell Survival.
846 *Developmental cell* **45**:170-182.e7. doi:10.1016/j.devcel.2018.03.022
- 847 Dmitrieff S, Nédélec F. 2015. Membrane Mechanics of Endocytosis in Cells with
848 Turgor. *PLoS Computational Biology* **11**. doi:10.1371/journal.pcbi.1004538
- 849 Evans E, Yeung a. 1989. Apparent viscosity and cortical tension of blood
850 granulocytes determined by micropipet aspiration. *Biophysical journal* **56**:151–
851 160. doi:10.1016/S0006-3495(89)82660-8
- 852 Ferguson JP, Huber SD, Willy NM, Aygün E, Goker S, Atabey T, Kural C. 2017.
853 Mechanoregulation of clathrin-mediated endocytosis. *Journal of Cell Science*
854 **130**:3631–3636. doi:10.1242/jcs.205930
- 855 Ferguson S, Raimondi A, Paradise S, Shen H, Mesaki K, Ferguson A, Destaing O,
856 Ko G, Takasaki J, Cremona O, O' Toole E, De Camilli P. 2009. Coordinated
857 Actions of Actin and BAR Proteins Upstream of Dynamin at Endocytic
858 Clathrin-Coated Pits. *Developmental Cell* **17**:811–822.
859 doi:10.1016/j.devcel.2009.11.005
- 860 Flor-Parra I, Zhurinsky J, Bernal M, Gallardo P, Daga RR. 2014. A Lallzyme MMX-
861 based rapid method for fission yeast protoplast preparation. *Yeast* **31**:61–66.
862 doi:10.1002/yea.2994
- 863 Gachet Y, Hyams JS. 2005. Endocytosis in fission yeast is spatially associated with
864 the actin cytoskeleton during polarised cell growth and cytokinesis. *Journal of*
865 *Cell Science* **118**:4231–4242. doi:10.1242/jcs.02530
- 866 Gauthier NC, Rossier OM, Mathur A, Hone JC, Sheetz MP. 2009. Plasma Membrane
867 Area Increases with Spread Area by Exocytosis of a GPI-anchored Protein
868 Compartment. *Molecular Biology of the Cell* **20**:3261–3272.
869 doi:10.1091/mbc.e09-01-0071
- 870 Hassinger JE, Oster G, Drubin DG, Rangamani P. 2017. Design principles for robust
871 vesiculation in clathrin-mediated endocytosis. *Proceedings of the National*
872 *Academy of Sciences* **114**:E1118–E1127. doi:10.1073/pnas.1617705114
- 873 Hohmann S. 2015. An integrated view on a eukaryotic osmoregulation system.
874 *Current Genetics* **61**:373–382. doi:10.1007/s00294-015-0475-0
- 875 Hohmann S. 2002. Osmotic Stress Signaling and Osmoadaptation in Yeasts
876 Osmotic. *Microbiology and Molecular Biology Reviews* **66**:300–372.
877 doi:10.1128/MMBR.66.2.300
- 878 Homann U. 1998. Fusion and fission of plasma-membrane material accommodates
879 for osmotically induced changes in the surface area of guard-cell protoplasts.
880 *Planta* **206**:329–333. doi:10.1007/s004250050408

- 881 Kabeche R, Baldissard S, Hammond J, Howard L, Moseley JB. 2011. The filament-
882 forming protein Pil1 assembles linear eisosomes in fission yeast. *Molecular*
883 *Biology of the Cell* **22**:4059–4067. doi:10.1091/mbc.E11-07-0605
- 884 Kabeche R, Howard L, Moseley JB. 2015. Eisosomes provide membrane reservoirs
885 for rapid expansion of the yeast plasma membrane. *Journal of Cell Science*
886 **128**:4057–4062. doi:10.1242/jcs.176867
- 887 Lacy MM, Baddeley D, Berro J, Lidke D. 2017. Single-molecule imaging of the BAR-
888 domain protein Pil1p reveals filament-end dynamics. *MBoC* **28**:2251–2259.
889 doi:10.1091/mbc.e17-04-0238
- 890 Lacy MM, Ma R, Ravindra NG, Berro J. 2018. Molecular mechanisms of force
891 production in clathrin-mediated endocytosis. *FEBS Letters*. doi:10.1002/1873-
892 3468.13192
- 893 Lo HP, Hall TE, Parton RG. 2016. Mechanoprotection by skeletal muscle caveolae.
894 *BioArchitecture* **0992**:00–00. doi:10.1080/19490992.2015.1131891
- 895 Lo Presti L, Chang F, Martin SG. 2012. Myosin Vs organize actin cables in fission
896 yeast. *Molecular Biology of the Cell*. doi:10.1091/mbc.E12-07-0499
- 897 Ma R, Berro J. 2020. Endocytosis against high turgor pressure is made easier by
898 partial protein coating and a freely rotating base. *bioRxiv* 558890.
899 doi:10.1101/558890
- 900 Minc N, Boudaoud A, Chang F. 2009. Mechanical forces of fission yeast growth.
901 *Current biology*: *CB* **19**:1096–1101. doi:10.1016/j.cub.2009.05.031
- 902 Morris CE, Homann U. 2001. Cell Surface Area Regulation and Membrane Tension.
903 *The Journal of Membrane Biology* **179**:79–102. doi:10.1007/s002320010040
- 904 Moseley JB. 2018. Eisosomes. *Current Biology* **28**:R376–R378.
905 doi:10.1016/J.CUB.2017.11.073
- 906 Mostov KE, Verges M, Altschuler Y. 2000. Membrane traffic in polarized epithelial
907 cells. *Current Opinion in Cell Biology* **12**:483–490. doi:10.1016/S0955-
908 0674(00)00120-4
- 909 Nicholson-Fish JC, Smillie KJ, Cousin MA. 2016. Monitoring activity-dependent bulk
910 endocytosis with the genetically-encoded reporter VAMP4-pHluorin. *Journal of*
911 *Neuroscience Methods* **266**:1–10. doi:10.1016/j.jneumeth.2016.03.011
- 912 Olivera-Couto A, Grana M, Harispe L, Aguilar PS. 2011. The eisosome core is
913 composed of BAR domain proteins. *Molecular Biology of the Cell* **22**:2360–
914 2372. doi:10.1091/mbc.E10-12-1021
- 915 Palmer SE, Smaczynska-de Rooij II, Marklew CJ, Allwood EG, Mishra R, Johnson S,
916 Goldberg MW, Ayscough KR. 2015. A dynamin-actin interaction is required for
917 vesicle scission during endocytosis in yeast. *Current Biology* **25**:868–878.
918 doi:10.1016/j.cub.2015.01.061
- 919 Parton RG, Pozo MA del, Vassilopoulos S, Nabi IR, Lay SL, Lundmark R, Kenworthy
920 AK, Camus A, Blouin CM, Sessa WC, Lamaze C. 2019. Caveolae: The FAQs.
921 *Traffic n/a*. doi:10.1111/tra.12689
- 922 Richards DA, Guatimosim C, Betz WJ. 2000. Two Endocytic Recycling Routes
923 Selectively Fill Two Vesicle Pools in Frog Motor Nerve Terminals. *Neuron*
924 **27**:551–559. doi:10.1016/S0896-6273(00)00065-9
- 925 Riggi M, Bourgoignat C, Macchione M, Matile S, Loewith R, Roux A. 2019. TORC2
926 controls endocytosis through plasma membrane tension. *The Journal of Cell*
927 *Biology*. doi:10.1083/jcb.201901096
- 928 Riggi M, Niewola-Staszewska K, Chiaruttini N, Colom A, Kusmider B, Mercier V,
929 Soleimanpour S, Stahl M, Matile S, Roux A, Loewith R. 2018. Decrease in
930 plasma membrane tension triggers PtdIns(4,5)P2 phase separation to

- 931 inactivate TORC2. *Nature Cell Biology* **20**:1043–1051. doi:10.1038/s41556-
932 018-0150-z
- 933 Schaber J, Adrover MÀ, Eriksson E, Pelet S, Petelenz-Kurdziel E, Klein D, Posas F,
934 Goksör M, Peter M, Hohmann S, Klipp E. 2010. Biophysical properties of
935 *Saccharomyces cerevisiae* and their relationship with HOG pathway
936 activation. *European Biophysics Journal* **39**:1547–1556. doi:10.1007/s00249-
937 010-0612-0
- 938 Schindelin J, Arganda-Carreras I, Frise E, Kaynig V, Longair M, Pietzsch T, Preibisch
939 S, Rueden C, Saalfeld S, Schmid B, Tinevez JY, White DJ, Hartenstein V,
940 Eliceiri K, Tomancak P, Cardona A. 2012. Fiji: An open-source platform for
941 biological-image analysis. *Nature Methods*. doi:10.1038/nmeth.2019
- 942 Schneider CA, Rasband WS, Eliceiri KW. 2012. NIH Image to ImageJ: 25 years of
943 image analysis. *Nature Methods* **9**:671–675. doi:10.1038/nmeth.2089
- 944 Sens P, Turner MS. 2006. Budded membrane microdomains as tension regulators.
945 *Physical Review E - Statistical, Nonlinear, and Soft Matter Physics* **73**:1–4.
946 doi:10.1103/PhysRevE.73.031918
- 947 Sinha B, Köster D, Ruez R, Gonnord P, Bastiani M, Abankwa D, Stan R V., Butler-
948 Browne G, Védie B, Johannes L, Morone N, Parton RG, Raposo G, Sens P,
949 Lamaze C, Nassoy P. 2011. Cells respond to mechanical stress by rapid
950 disassembly of caveolae. *Cell* **144**:402–413. doi:10.1016/j.cell.2010.12.031
- 951 Sirotkin V, Berro J, Macmillan K, Zhao L, Pollard TD. 2010. Quantitative analysis of
952 the mechanism of endocytic actin patch assembly and disassembly in fission
953 yeast. *Molecular biology of the cell* **21**:2894–904. doi:10.1091/mbc.E10-02-
954 0157
- 955 Skau CT, Courson DS, Bestul AJ, Winkelman JD, Rock RS, Sirotkin V, Kovar DR.
956 2011. Actin filament bundling by fimbrin is important for endocytosis,
957 cytokinesis, and polarization in fission yeast. *The Journal of biological*
958 *chemistry* **286**:26964–77. doi:10.1074/jbc.M111.239004
- 959 Smith CB, Betz WJ. 1996. Simultaneous independent measurement of endocytosis
960 and exocytosis. *Nature* **380**:531–534. doi:10.1038/380531a0
- 961 Stachowiak MR, Laplante C, Chin HF, Guirao B, Karatekin E, Pollard TD,
962 O’Shaughnessy B. 2014. Mechanism of cytokinetic contractile ring constriction
963 in fission yeast. *Developmental cell* **29**:547–61.
964 doi:10.1016/j.devcel.2014.04.021
- 965 Suarez C, Carroll RT, Burke TA, Christensen JR, Bestul AJ, Sees JA, James ML,
966 Sirotkin V, Kovar DR. 2015. Profilin Regulates F-Actin Network Homeostasis
967 by Favoring Formin over Arp2/3 Complex. *Developmental Cell* **32**:43–53.
968 doi:10.1016/J.DEVCEL.2014.10.027
- 969 Suescún-Bolívar LP, Thomé PE. 2015. Osmosensing and osmoregulation in
970 unicellular eukaryotes. *World Journal of Microbiology and Biotechnology*
971 **31**:435–443. doi:10.1007/s11274-015-1811-8
- 972 Tinevez JY, Perry N, Schindelin J, Hoopes GM, Reynolds GD, Laplantine E,
973 Bednarek SY, Shorte SL, Eliceiri KW. 2017. TrackMate: An open and
974 extensible platform for single-particle tracking. *Methods* **115**:80–90.
975 doi:10.1016/j.ymeth.2016.09.016
- 976 Urbina FL, Gomez SM, Gupton SL. 2018. Spatiotemporal organization of exocytosis
977 emerges during neuronal shape change. *Journal of Cell Biology* **217**:1113–
978 1128. doi:10.1083/jcb.201709064
- 979 Vida T, Gerhardt B. 1999. A Cell-Free Assay Allows Reconstitution of Vps33p-
980 Dependent Transport to the Yeast Vacuole/Lysosome. *J Cell Biol* **146**:85–98.

- 981 Vida TA, Emr SD. 1995. A new vital stain for visualizing vacuolar membrane
982 dynamics and endocytosis in yeast. *The Journal of cell biology* **128**:779–92.
983 doi:10.1083/JCB.128.5.779
- 984 Walther TC, Aguilar PS, Fröhlich F, Chu F, Moreira K, Burlingame AL, Walter P.
985 2007. Pkh-kinases control eisosome assembly and organization. *The EMBO*
986 *journal* **26**:4946–55. doi:10.1038/sj.emboj.7601933
- 987 Watanabe S, Boucrot E. 2017. Fast and ultrafast endocytosis. *Current Opinion in Cell*
988 *Biology* **47**:64–71. doi:10.1016/j.ceb.2017.02.013
- 989 Ziólkowska NE, Karotki L, Rehman M, Huisken JT, Walther TC. 2011. Eisosome-
990 driven plasma membrane organization is mediated by BAR domains. *Nature*
991 *structural & molecular biology* **18**:854–856. doi:10.1038/nsmb.2080
992

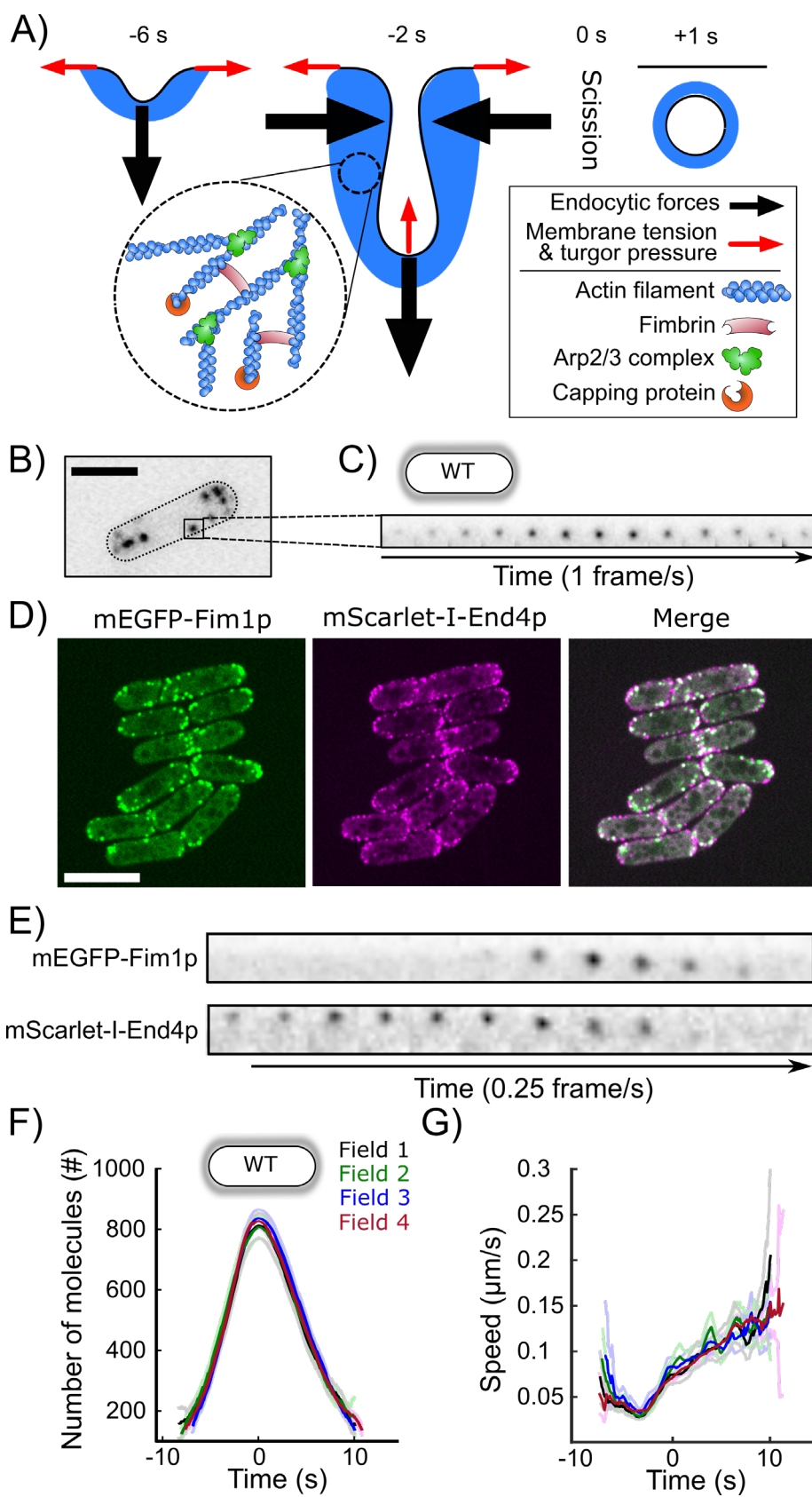


Figure 1: Quantitative measurements of fimbrin dynamics at sites of clathrin-mediated endocytosis are highly reproducible. A) Schematic of the plasma membrane deformations and the main components of the actin machinery during CME. Fimbrin (Fim1p, red) crosslinks actin filaments (blue) present at endocytic sites and is used as a proxy to monitor the amount of actin assembled. B) Wild-type yeast cell expressing Fim1p-mEGFP (inverted contrast). C) Montage of a representative CME event. The interval between each frame is 1 s. D) Colocalization of Fimbrin (mEGFP-Fim1p, green) and End4 (mScarlet-I-End4p, red) during endocytosis. Significant overlapping of signals can be seen in the merged channel. E) Montage of a representative CME event tagged by both mEGFP-Fim1p (top-row) and mScarlet-I-End4p (bottom row). The interval between each frame is 4 s. F) and G) The number of molecules (F) and speed (G) of Fim1p-mEGFP detected, tracked and aligned with temporal super-resolution (Berro & Pollard, 2014) is highly reproducible between fields of view (one-way ANOVA on the number of molecules at time 0 s, $p=0.74$). Each curve with a dark color represents the average of several endocytic events from a different field of view of the same sample ($N \geq 64$), and the light colors are the 95% confidence intervals. For each average curve, the peak value corresponds to time 0 sec, when vesicles scission happens. The data for each field are plotted separately in Figure 1 Supplement 1. The numbers of endocytic events used in each curve are given in Supplemental Table 2. Scale bars in (B) and (F): 5 μm .

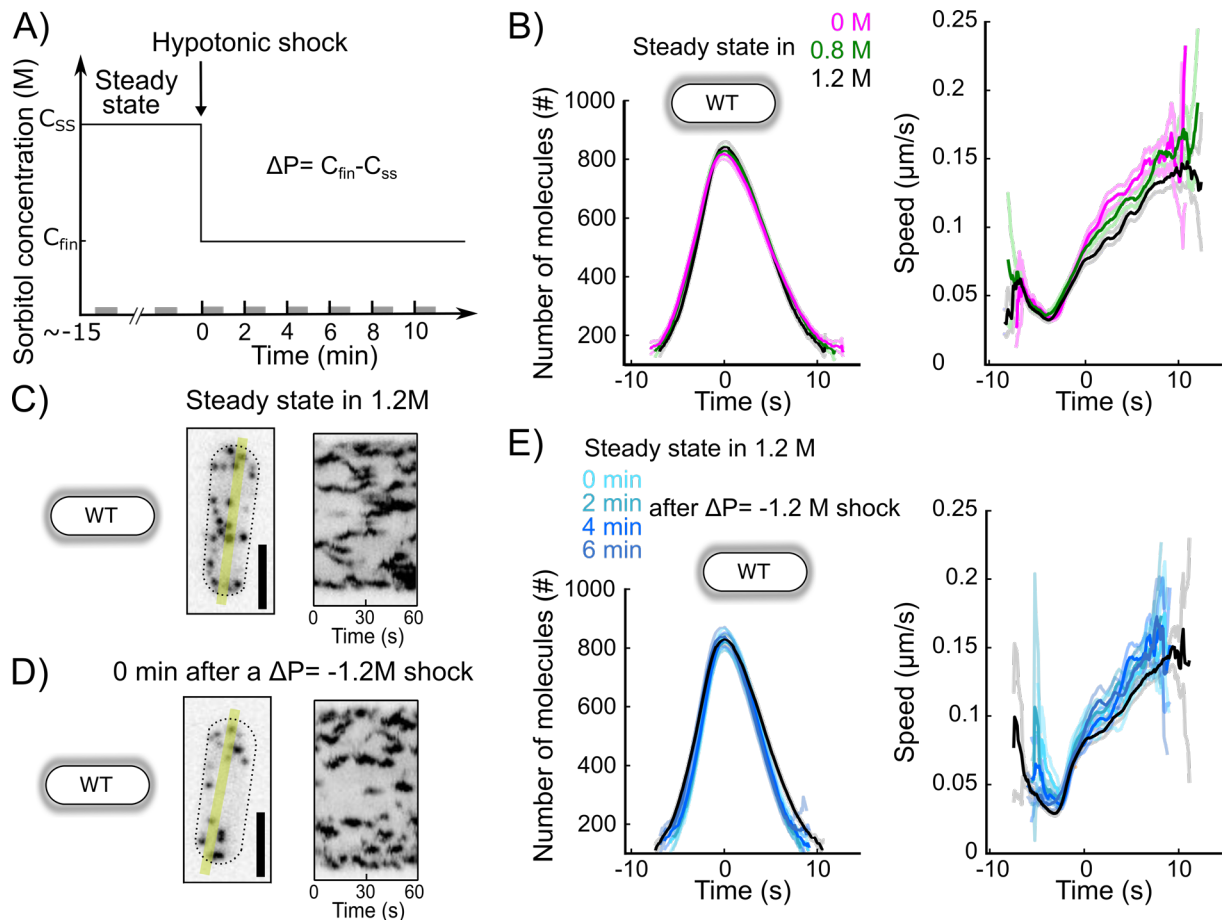


Figure 2: CME in wild-type walled cells is robust over a wide range of osmotic conditions. A) Timeline of the experiments and notations. By convention, hypotonic shocks start at time 0 min and are defined by the difference in concentration of sorbitol in the steady state media before the shock (C_{ss}) and after the hypotonic shock (C_{fin}), $\Delta P = C_{fin} - C_{ss}$. Data for a given time point correspond to endocytic events happening within 1 minute after this time point (e.g. the data at $t=0$ min correspond to endocytic events happening between 0 and 1 min after the shock). These time intervals are represented by gray bars on the time axis. B) Number of molecules (left panel) and speed (right panel) of Fim1p-mEGFP in wild-type walled cells at steady state in media supplemented with different sorbitol concentrations. There is no statistically significant difference in the number of molecules at time 0 s between the three conditions (one-way ANOVA, $p=0.29$). $N \geq 388$. Data for each condition are plotted separately in Figure 2 Supplement 1A. The numbers of endocytic events used in each curve are given in Supplemental Table 3. C) and D) Left panels: representative wild-type walled cells expressing Fim1p-mEGFP (inverted contrast) at steady state in 1.2 M sorbitol (D) and immediately (0 min) after an acute osmotic shock $\Delta P = -1.2$ M (E). Right panels: kymographs of the fluorescence under the yellow line in the left panels. Black dashed lines: outline of the cell. Scale bars for all panels: 5 μm . E) Number of molecules (left panel) and speed (right panel) of Fim1p-mEGFP for wild-type walled cells initially at steady state in 1.2 M sorbitol and after an acute osmotic shock of $\Delta P = -1.2$ M. There is no statistically significant difference in the number of molecules at time 0 s between the three conditions (one-way ANOVA, $p=0.95$). Black: steady state in 1.2 M sorbitol; light to dark blue in top panel: 0 min, 2 min, 4 min, and 6 min after the acute hypotonic

under a [CC-BY-NC-ND 4.0 International license](#).
shock ($N \geq 103$). Data for each condition are plotted separately in Figure 2 Supplement 1B. The numbers of endocytic events used in each curve are given in Supplemental Table 4. (B) and (E): dark colors: average; light colors: average \pm 95% confidence interval.

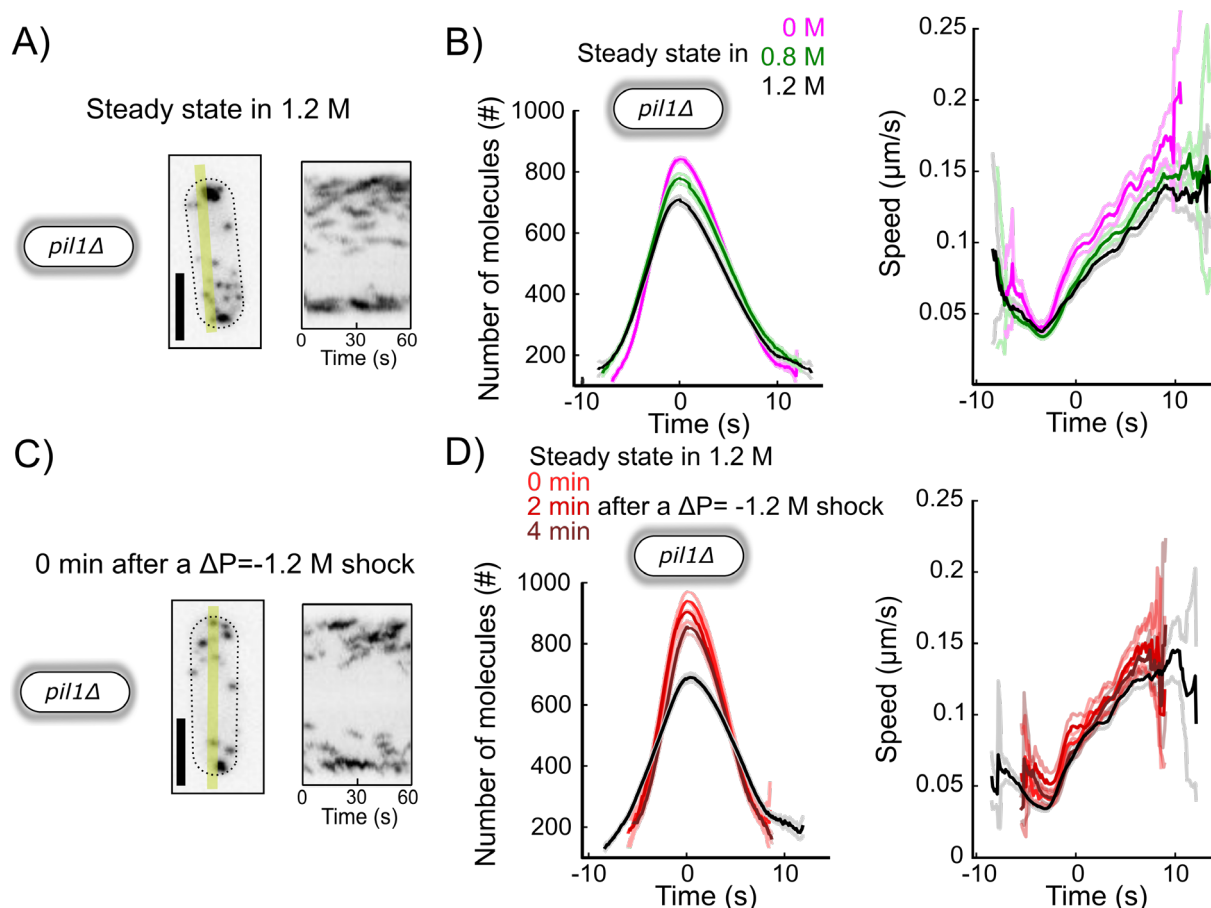


Figure 3: The absence of eisosome makes the dynamics of the CME machinery more sensitive to changes in osmolarity. A) and C) Left panels: representative *pil1Δ* walled cells expressing Fim1p-mEGFP (inverted contrast) at steady state in 1.2 M sorbitol (A) and immediately (0 min) after an acute osmotic shock of $\Delta P = -1.2$ M (C). Right panels: kymographs of the fluorescence under the yellow lines in the left panels. Black dashed lines: cell outline. Scale bars: 5 μm . B) Number of molecules (left panel) and speed (right panel) of Fim1p-mEGFP in *pil1Δ* walled cells at steady state in media supplemented with different sorbitol concentrations ($N \geq 342$). The difference in the number of molecules at time 0 s between all pairs of conditions is statistically significant (one-way ANOVA, $p < 10^{-5}$). Data for each condition are plotted separately in Figure 3 Supplement 1A. The numbers of endocytic events used in each curve are given in Supplemental Tables 5. D) Number of molecules (left panel) and speed (right panel) of Fim1p-mEGFP in *pil1Δ* walled cells before and after an acute osmotic shock ($\Delta P = -1.2$ M). The difference in the number of molecules at time 0 s between all pairs of conditions is statistically significant (one-way ANOVA, $p < 0.03$) except between 0 min and 2 min after the shock (one-way ANOVA, $p = 0.18$). Black: steady state in 1.2 M sorbitol before the hypotonic shock ($N = 583$); light to dark red in top panel: 0 min, 2 min and 4 min after the acute hypotonic shock ($N \geq 145$). Data for each condition are plotted separately in Figure 3 Supplement 1B. The numbers of endocytic events used in each curve are given in Supplemental Table 6. (B) and (D): dark colors: average; light colors: average \pm 95% confidence interval.

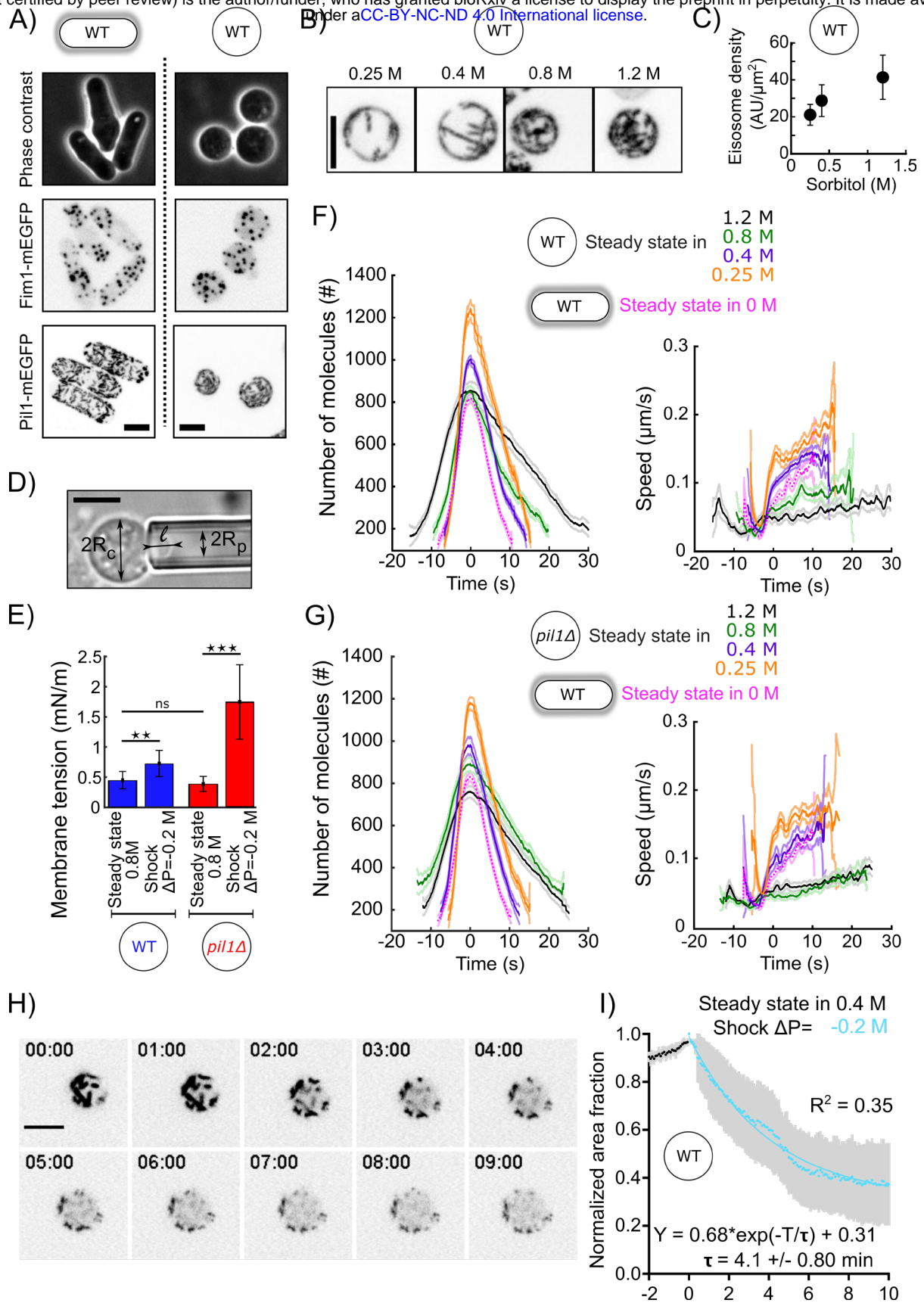


Figure 4: Eisosomes buffer increases in membrane tension but has virtually no influence on the dynamics of the actin endocytic machinery at steady state in protoplasts. A) Representative walled yeast cells (left column) and protoplasts (right column) at steady state in 1.2 M sorbitol. Top panels: phase contrast; middle panels: cells expressing Fim1-mEGFP (inverted contrast); bottom panels: cells expressing Pil1-mEGFP (inverted contrast). Note that the expression of pil1-mEGFP is the same in walled cells and protoplasts (Figure 4 Supplement 1). B) Eisosomes labelled with Pil1p-mEGFP (inverted contrast) in wild-type protoplasts at steady state in different sorbitol concentrations. From left to right: 0.25 M, 0.4 M, 0.8 M and 1.2 M sorbitol. C) Density of eisosomes at the plasma membrane, measured as the ratio between the intensity of Pil1p-mEGFP on the plasma membrane and the surface area of the protoplast, at steady state in 0.25 M (N=26), 0.4 M (N=34) and 1.2 M (N=39) sorbitol. Error bars: standard deviations. D) Micropipette aspiration was used to measure membrane tension. R_c : cell radius; R_p : micropipette radius; l : length of the tongue inside the micropipette. E) Membrane tension of protoplasts at steady state in 0.8 M sorbitol and ~ 5 min after a hypotonic shock ($\Delta P = -0.2$ M) for wild-type (blue bars, N=28 for steady state and N=5 for the shock) and *pil1* Δ protoplasts (red bars, N=42 for steady state and N=7 for the shock). Error bars: standard deviation. p-values: non-significant (ns), $p > 0.05$; two stars (**), $p \leq 0.01$; three stars (***), $p \leq 0.001$. F) and G) Number of molecules (left panels) and speed (right panels) of Fim1p-mEGFP for wild-type (F) and *pil1* Δ (G) protoplasts at steady state in different sorbitol concentrations. Orange: 0.25 M; purple: 0; green: 0.8 M; black: 1.2 M. Dark colors: average; light colors: average \pm 95% confidence interval (N \geq 143). Fuchsia dotted curves: wild-type walled cells at steady state in 0 M sorbitol. Data for each condition are plotted separately in Figure 4 Supplement 2. The numbers of endocytic events used in each curve are given in Supplemental Table 7. H) and I) Eisosomes of wild-type protoplasts disassemble rapidly after a hypotonic shock. (H) Time course of a representative protoplast expressing Pil1p-mEGFP over 10 minutes after a hypotonic shock ($\Delta P = -0.2$ M) and initially at steady-state in 0.4 M sorbitol (just before time 0 min). (I) Evolution of the surface area covered by eisosomes over time, as a fraction of the surface area covered at time 0 min (normalized to 1). Data are from three independent experiments (N=15) and presented as mean \pm 95% confidence interval. Scale bars in (A), (B), (D) and (I): 5 μ m.

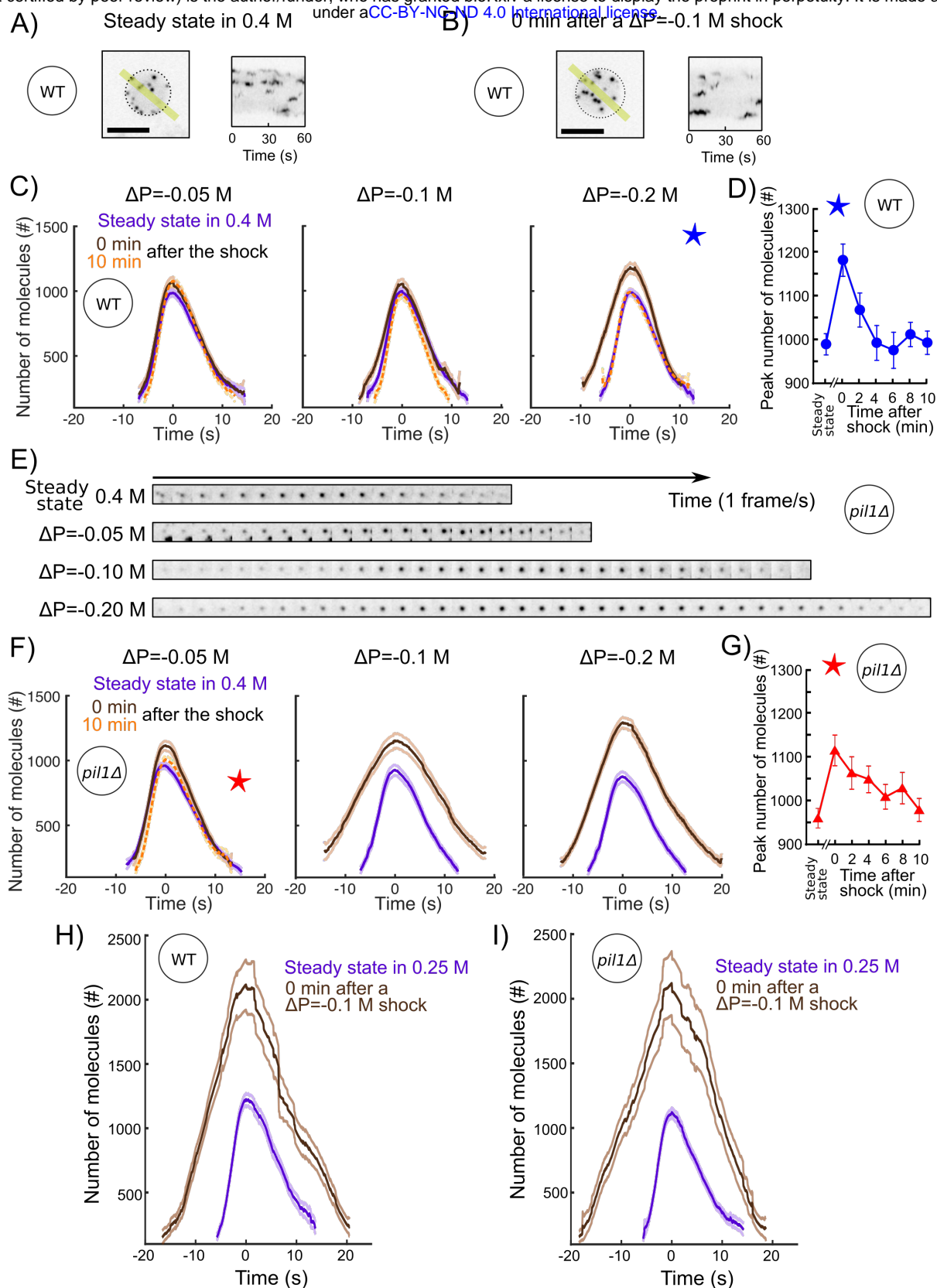


Figure 5: The actin endocytic machinery adapts to increases of membrane tension in protoplasts. A) and B) Representative wild-type protoplasts expressing Fim1-mEGFP (inverted contrast) at steady-state in 0.25 M sorbitol (A, left panel) and immediately after (0 min) an acute osmotic shock of $\Delta P = -0.1$ M (B, left panel). Right panels: kymographs of the fluorescence under the yellow lines in the left panels. Black dashed lines: protoplast outline. Scale bars: 5 μm . C) and F) Number of Fim1p-mEGFP molecules in wild-type (C) and *pil1* Δ (F) protoplasts at steady-state in 0.4 M sorbitol (purple), 0 min (brown) and 10 min (orange) after an hypotonic shock of $\Delta P = -0.05$ M (left panels), $\Delta P = -0.1$ M (middle panels) and $\Delta P = -0.2$ M (right panels), $N \geq 95$.

Data for each condition are plotted separately in Figure 5 Supplements 1 (wild type) and 2 (*pil1* Δ). The speeds of Fim1p-mEGFP for each condition are shown in Figure 5 Supplements 3 (wild type) and 4 (*pil1* Δ). The numbers of endocytic events used in each curve are given in Supplemental Table 8. Note that the large majority of *pil1* Δ protoplasts were too damaged or dead 2 minutes after hypotonic shocks larger than or equal to $\Delta P = -0.1$ M to allow us to track enough endocytic events and produce a curve (Figures 6B and C, Figure 6 Supplement 1). In panel (C), the difference in the number of molecules at time 0 s at steady state and 0 min after the shock is statistically significant for all shocks (one-way ANOVA, $p < 0.03$) and the difference between steady-state and 10 min after the shock is not statistically significant (one-way ANOVA, $p > 0.2$; details in the data file for figure 5C). In panel (F), the difference at steady state and 0 min after the shock is statistically significant for all shocks (one-way ANOVA, $p < 10^{-5}$; details in the data file for figure 5F). D) Temporal adaptation of the peak number of Fim1p-mEGFP in wild-type protoplasts initially at steady state in 0.4 M sorbitol and 0 to 10 min after a $\Delta P = -0.2$ M osmotic shock. The condition for this figure is the same as the condition with the blue star in (C). The difference between steady-state and 0 min or 2 min after shock is statistically significant (one-way ANOVA, $p < 10^{-3}$; details in the data file for figure 5D). The difference between steady-state and 4 min, 6 min, 8 min and 10 min after shock is not statistically significant (one-way ANOVA, $p > 0.2$; details in the data file for figure 5D). E) Montage of representative endocytic events (Fim1-mEGFP, inverted contrast) in *pil1* Δ protoplasts (1 frame per second) at steady state in 0.4 M sorbitol (first row) and immediately after (0 min) a hypotonic shocks of $\Delta P = -0.05$ M (second row), $\Delta P = -0.10$ M (third row) and $\Delta P = -0.20$ M (fourth row). G) Temporal adaptation of the peak number of Fim1p-mEGFP in *pil1* Δ protoplasts initially at steady state in 0.4 M sorbitol and 0 to 10 min after a $\Delta P = -0.05$ M shock. The condition in this figure is the same as the condition with the red star in (F). The difference between steady-state and 0 min, 2 min, 4 min, 6 min or 8 min after shock is statistically significant (one-way ANOVA, $p < 0.01$; details in the data file for figure 5F). The difference between steady-state and 10 min after shock is not statistically significant (one-way ANOVA, $p > 0.3$; details in the data file for figure 5F). (D) and (G) error bars are 95% confidence intervals. The numbers of endocytic events at each time point are given in Supplemental Table 9. H) and I) Number of molecules of Fim1p-mEGFP for wild-type (H) and *pil1* Δ (I) protoplasts at steady state in 0.25 M sorbitol (purple dashed) and immediately after (0 min) a hypotonic shock of $\Delta P = -0.1$ M (brown), $N \geq 67$. The difference in the number of molecules at time 0 s at steady state and 0 min after the shock is statistically significant for all conditions (one-way ANOVA, $p < 10^{-16}$). The speed data for each condition are plotted in Figure 5 Supplement 5. The numbers of endocytic events used in each curve are given in Supplemental Table 10. The survival rates for the wild-type and *pil1* Δ protoplasts in these conditions are plotted in Figure 5-

Supplement 5C.

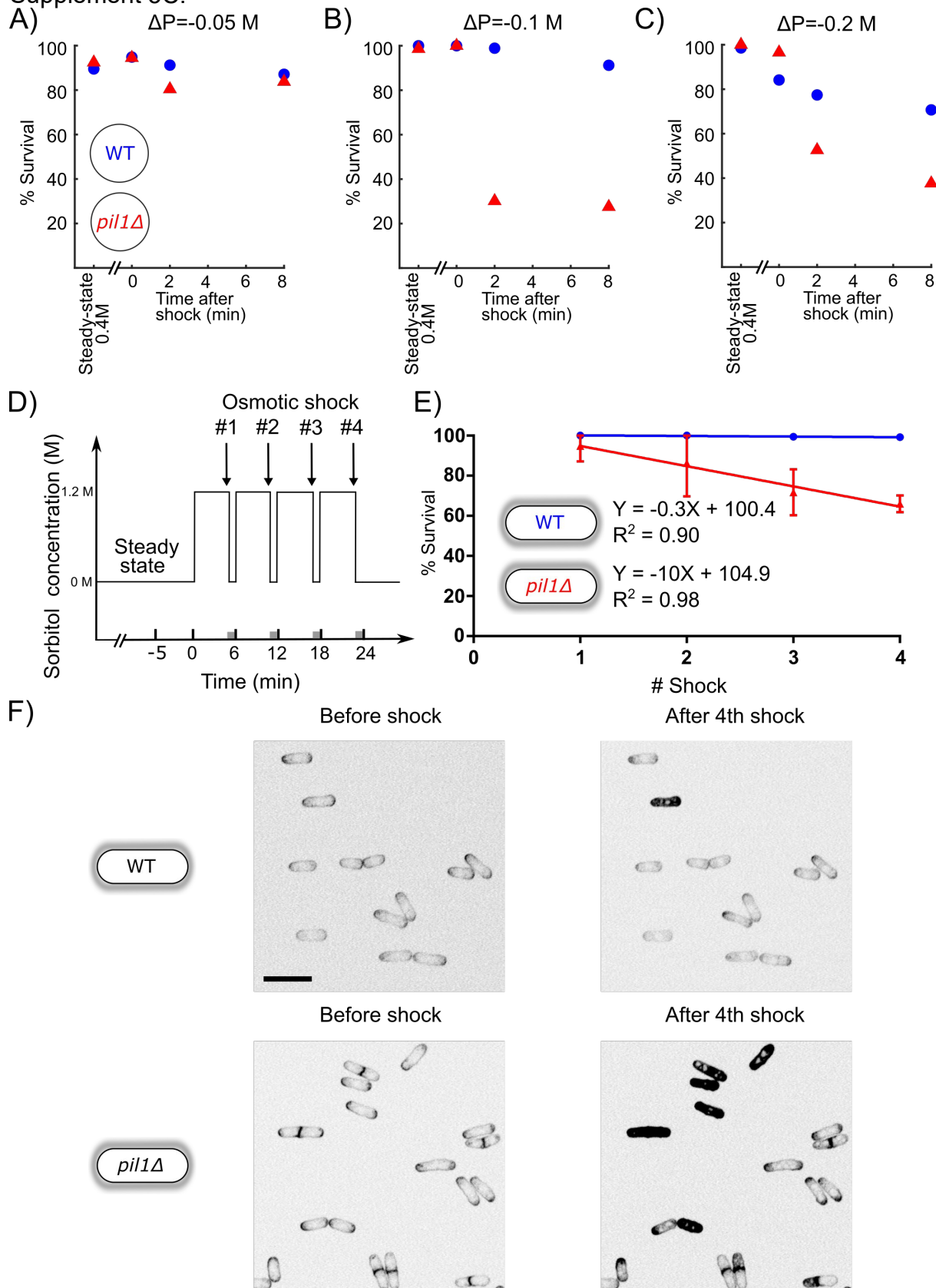


Figure 6: Eisosomes protect protoplasts and walled cells from osmotic shocks.

A-C) Percentage of wild-type (blue dots) and *pil1* Δ (red triangle) protoplasts that are alive at steady-state in 0.4 M sorbitol, and after a $\Delta P = -0.05$ M (A), $\Delta P = -0.1$ M (B) and $\Delta P = -0.2$ M (C) single hypotonic shock. Representative fields of view used to determine these percentages are shown in Figure 6 Supplement 1. D) Timeline of repeated $\Delta P = 1.2$ M osmotic shocks for walled cells. Each osmotic shock was performed by exchanging sorbitol concentration from 1.2 M (5 minutes) to 0 M (1 minute). E) Percentage of wild-type (blue dots, N=273) and *pil1* Δ (red triangle, N=197) walled cells that are alive after each osmotic shock. Note the progressive cell death induced by repeated osmotic shocks for *pil1* Δ cells. Combined data are from three independent experiments and plotted as mean \pm standard deviation. F) Representative images of wild-type (upper panel) and *pil1* Δ (lower panel) walled cells before shock and after the 4th shock. Dead cells are strongly stained by FM4-64 due to membrane damage. Scale bar: 10 μ m.

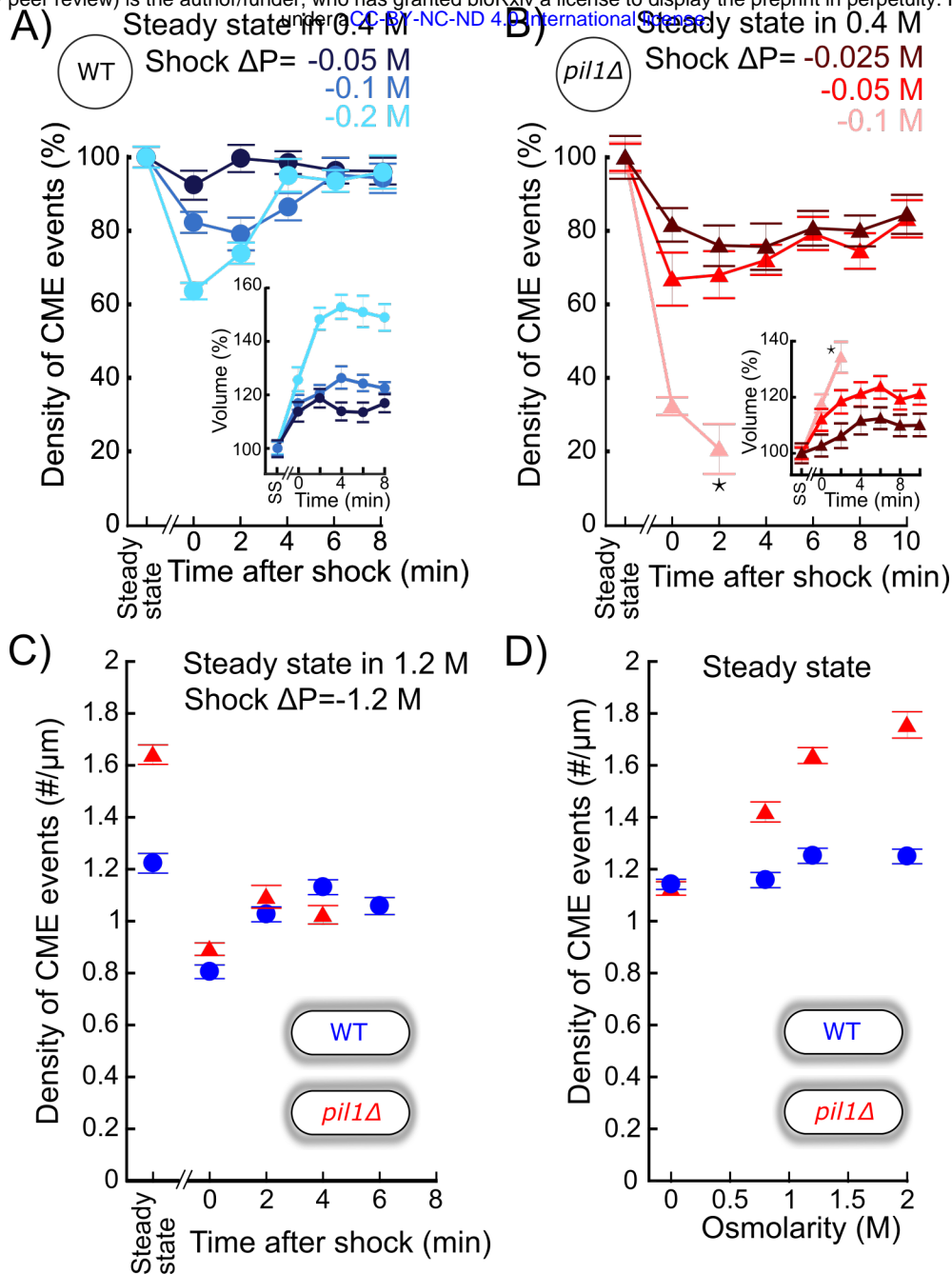


Figure 7: The density of endocytic events rapidly adapts after acute osmotic shocks. A) Temporal evolution of density of endocytic events (average number of endocytic events at a given time in a cell divided by the cell length) in wild-type protoplasts initially at steady state in 0.4 M sorbitol and after an acute hypotonic shock of $\Delta P = -0.05$ M (dark blue, $N_{\text{cell}} \geq 102$), $\Delta P = -0.1$ M (blue, $N_{\text{cell}} \geq 54$) and $\Delta P = -0.2$ M (light blue, $N_{\text{cell}} \geq 83$). For $\Delta P = -0.1$ M and $\Delta P = -0.2$ M, the difference in the density of CME events between steady-state and 0 min or 2 min after the shock is statistically significant (one-way ANOVA, $p < 10^{-4}$). In all conditions, the difference after 6 min is not significant (one-way ANOVA, $p > 0.12$; details in the data file). B) Same as (A) but with *pil1* Δ protoplasts and hypotonic shocks of $\Delta P = -0.025$ M (dark red, $N_{\text{cell}} \geq 70$), $\Delta P = -0.05$ M (red, $N_{\text{cell}} \geq 103$) and $\Delta P = -0.1$ M (light red, $N_{\text{cell}} \geq 78$). In all conditions, the difference in the density of CME events between steady-state and any time after the shock is statistically significant (one-way ANOVA, $p < 10^{-3}$). For $\Delta P = -0.025$ M and $\Delta P = -0.05$ M,

the differences between time points after 6 min are not significant (one-way ANOVA, $p > 0.09$; details in the data file). (A) and (B) insets: relative volume increase after the hypotonic shocks (the volume at steady state is used as a reference). The numbers of cells used for each condition and each time point are given in Supplemental Table 11. The number of cells measured in the insets are the same as in the main figures. Star (*): the large majority of *pil1* Δ protoplasts were too damaged or dead 4 minutes after the hypotonic shocks at $\Delta P = -0.1$ M (Figure 6B), which prevented us to measure the density of endocytic events and the volume after this time point. C) Density of endocytic events in wild-type (blue circle) and *pil1* Δ (red triangle) walled cells initially at steady state in 1.2 M sorbitol and after an acute hypotonic shock of $\Delta P = -1.2$ M, $N_{\text{cell}} \geq 44$. The numbers of cells used for each condition and each time point are given in Supplemental Table 12. For wild-type and *pil1* Δ walled cells, the differences in the density of CME events after 2 min are not statistically significant ($p > 0.08$; details in the data file). D) Density of endocytic events in intact cells at steady state in different osmolarities, $N_{\text{cell}} \geq 80$. In *pil1* Δ walled cells, the difference in the density of CME events between all pairs of conditions is statistically significant (one-way ANOVA, $p < 10^{-4}$). In wild-type walled cells, the difference is small but statistically significant (details in the data file). (A), (B), (C) and (D): error bars are standard errors of the mean. The numbers of cells used for each condition and each time point are given in Supplemental Table 13.

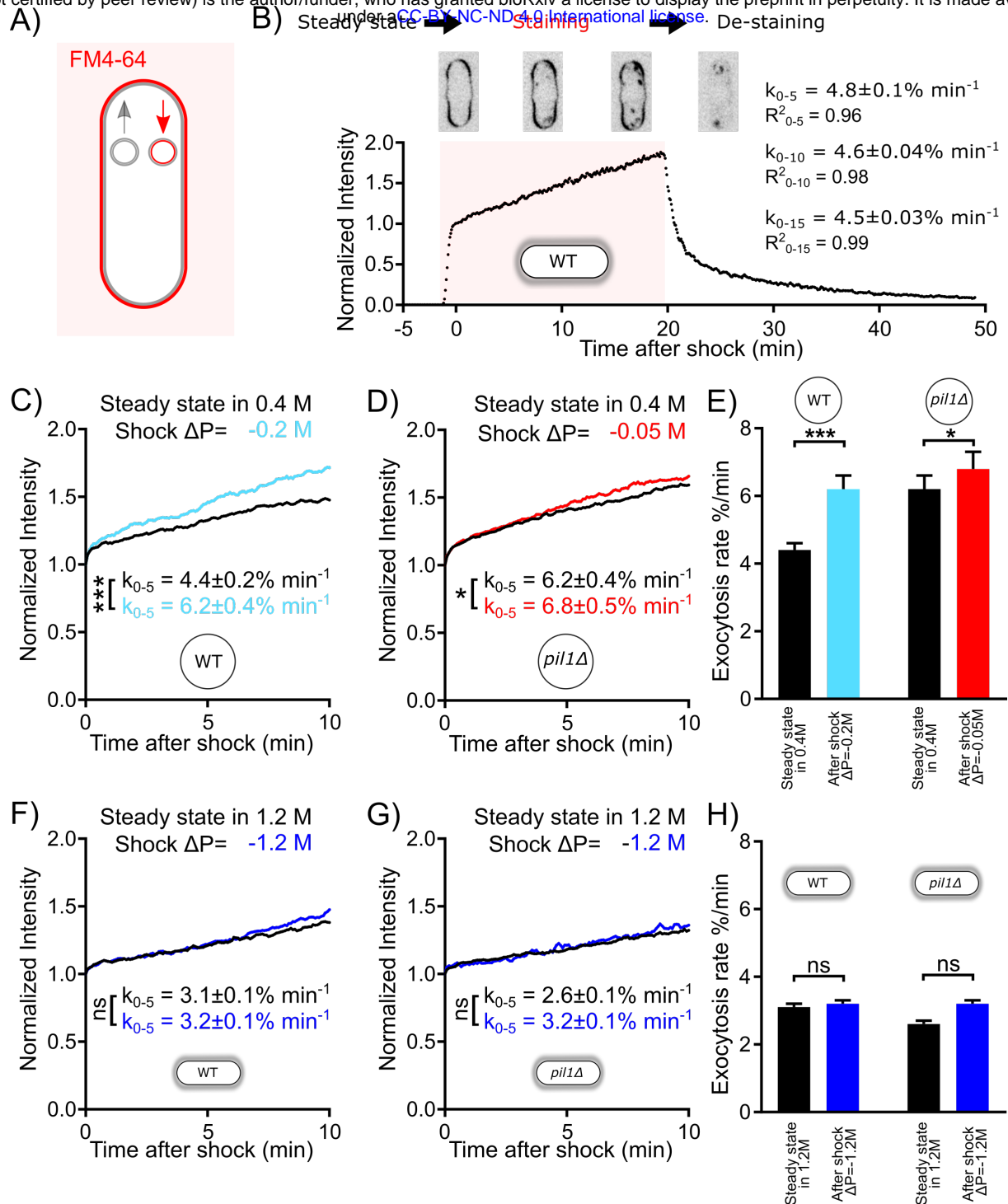


Figure 8: Exocytosis rate increases after an acute change in membrane tension in protoplasts but not in walled cells. A) Rationale of measurement of whole cell exocytosis rate through FM4-64 staining. After FM4-64 is flown in the imaging chamber, the dye rapidly binds to the cell surface in less than a minute. After this initial phase, the whole cell fluorescence increases every time new (unlabeled) internal membrane is exposed to the cell surface by exocytosis. Note that endocytic events do not change the total fluorescence measured. B) Measurement of yeast cell exocytosis rate at steady state in 0 M sorbitol. Cells were stained with 20 μM FM4-64 in EMM5S for 20 min before washing with EMM5S. During FM4-64 staining, the fluorescence intensity increases rapidly for 1 min before entering a slow linear phase over at least

under aCC-BY-NC-ND 4.0 International license.

20 min for wild-type cells. The fluorescence intensity at the end of the initial rapid increase phase corresponds to the complete staining of cell surface. It was normalized to 1, so that the subsequent increase in fluorescence intensity corresponds to a percentage of the plasma membrane surface area. After the dye was removed 20 min later, the decrease in fluorescence intensity suggests that the incorporation of FM4-64 didn't interfere with the vesicle trafficking pathway of the cell. The rate of exocytosis (measured as a percentage of the plasma membrane surface area per minute) is the slope of a linear fit of the measured signal over the first 5 min (k_{0-5}), 10 min (k_{0-10}) or 15 min (k_{0-15}). Example images of stained cells at different time points are shown in the middle panel (inverted contrast). (C) - (H) Rates of exocytosis at steady state and after hypotonic shocks. (C) and (D) The exocytic rate of wild-type and *pil1* Δ protoplasts increases after a $\Delta P = -0.2$ M (black, before shock, $N_{\text{cells}} = 20$; light blue, after shock, $N_{\text{cells}} = 37$; 4 replicates each) and $\Delta P = -0.05$ M (black, before shock, $N_{\text{cells}} = 44$; red, after shock, $N_{\text{cells}} = 60$; 4 replicates each) acute hypotonic shocks, respectively. Before time 0 min, all protoplasts were at steady-state in 0.4 M sorbitol. Curves for individual conditions in panels (C) and (D) are plotted in Figure 8 Supplement 1A and B, respectively. (E) Summary of exocytic rates for wild-type and *pil1* Δ protoplasts before and after hypotonic shock. (F) and (G) The exocytic rate of wild-type walled cells is not changed after a $\Delta P = -1.2$ M acute hypotonic shock (black, before shock, $N_{\text{cells}} = 79$; blue, after shock, $N_{\text{cells}} = 68$; 3 replicates each). The exocytic rate of *pil1* Δ walled cells does not change significantly in the same conditions (black, before shock, $N_{\text{cells}} = 60$; blue, after shock, $N_{\text{cells}} = 96$; 3 replicates each). All walled cells were at steady-state in 1.2 M sorbitol before time 0 min. Curves for individual conditions in panels (F) and (G) are plotted in Figure 8 Supplement 1C and D, respectively. (H) Summary of exocytic rates for wild-type and *pil1* Δ walled cells before and after hypotonic shock. (C) - (H) Data from at least three independent experiments were pooled together to produce each curve. p-values: non-significant (ns), $p > 0.05$; one star (*), $p \leq 0.05$; three stars (***), $p \leq 0.001$.

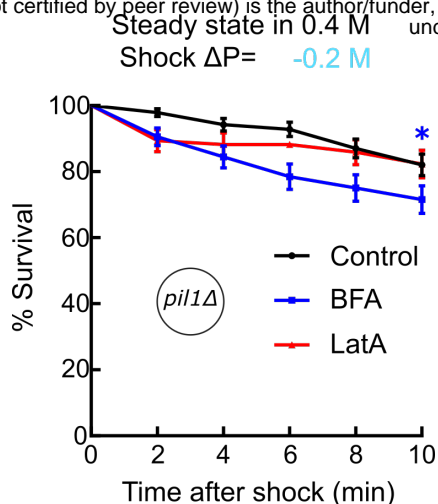
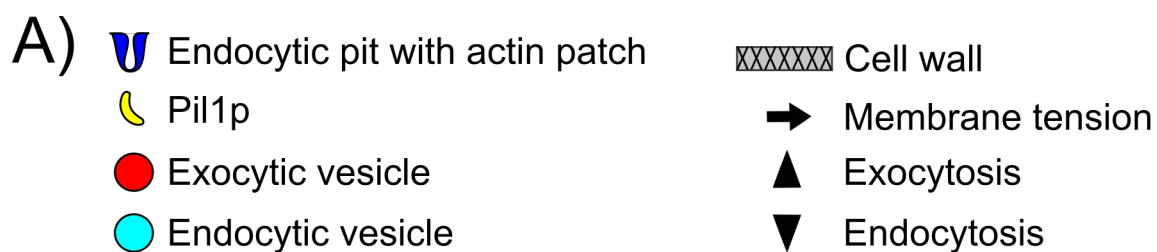









Figure 9: Inhibition of exocytosis but not endocytosis decreased the survival rate of protoplasts under acute hypotonic shock. *pil1* Δ protoplasts initially at steady state in 0.4 M sorbitol (black line; N=114), 0.4 M sorbitol plus 2 mM BFA (Blue line; N=83), or 0.4 M sorbitol plus 25 μ M Latrunculin A (Red line; N=70), were submitted to a $\Delta P = -0.2$ M hypotonic shock (t=0 min), and their survival rates were compared over time. BFA or Latrunculin A were included in the respective shock solution. Only BFA treatment led to a significant decreased survival rate of protoplasts compared with the control group. Data are pooled from two independent experiments and plotted as Kaplan-Meier survival curves. Error bars: standard error of the mean by the Greenwood formula. One star (*), $p \leq 0.05$, logrank test. Typical fields of view for each condition are shown in Figure 9 Supplement 1.

- A)  Endocytic pit with actin patch
 Pil1p
 Exocytic vesicle
 Endocytic vesicle
 Cell wall
 Membrane tension
 Exocytosis
 Endocytosis

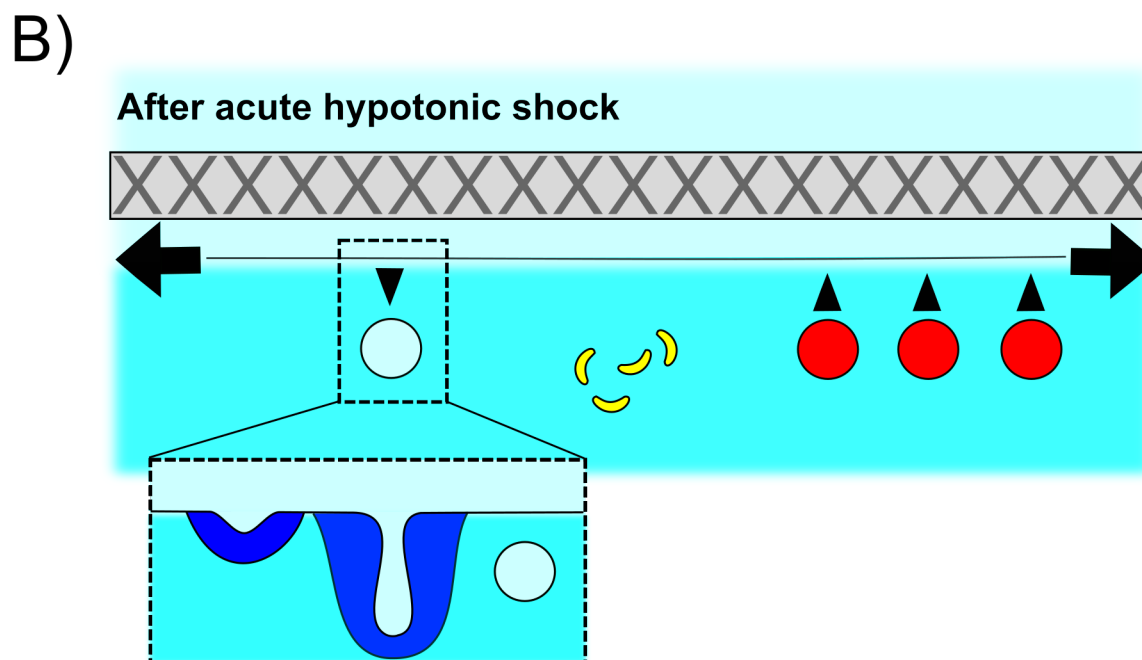
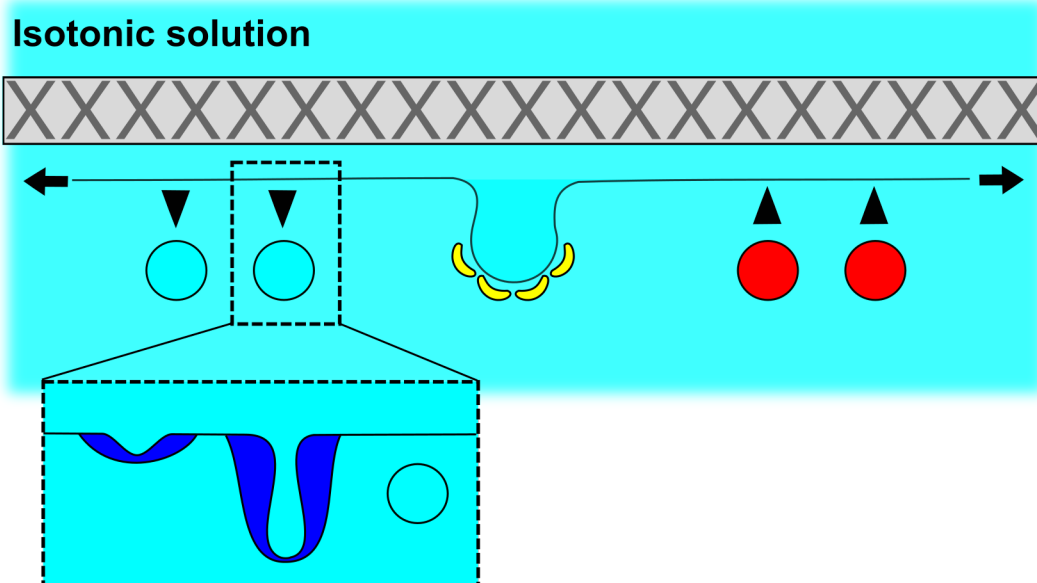


Figure 10: Schematic of the adaptation of fission yeast endocytosis, exocytosis and eisosome after acute hypotonic shock-induced increase in membrane tension. A) In an isotonic solution, endocytosis and exocytosis rates are largely balanced, and proteins including Pil1p are assembled at the plasma membrane to form eisosomes. Actin is recruited to endocytic sites to provide the forces needed to reshape the membrane under normal membrane tension. When present, cell wall makes fission yeast cell resistant to significant changes in the osmolarity of extracellular solution. B) Acute hypotonic shock results in an increase of membrane tension, which leads to a decrease of endocytosis rate, an increase in exocytosis rate, and a rapid disassembly of eisosomes, within ~2 minutes. The proteins of the actin machinery are recruited in larger amount to endocytic sites to provide larger forces for successful endocytosis under increased membrane tension. Failure of adaptation to the increase in membrane tension leads to membrane rupture and cell death in both protoplasts and walled cells.

Supplemental figures

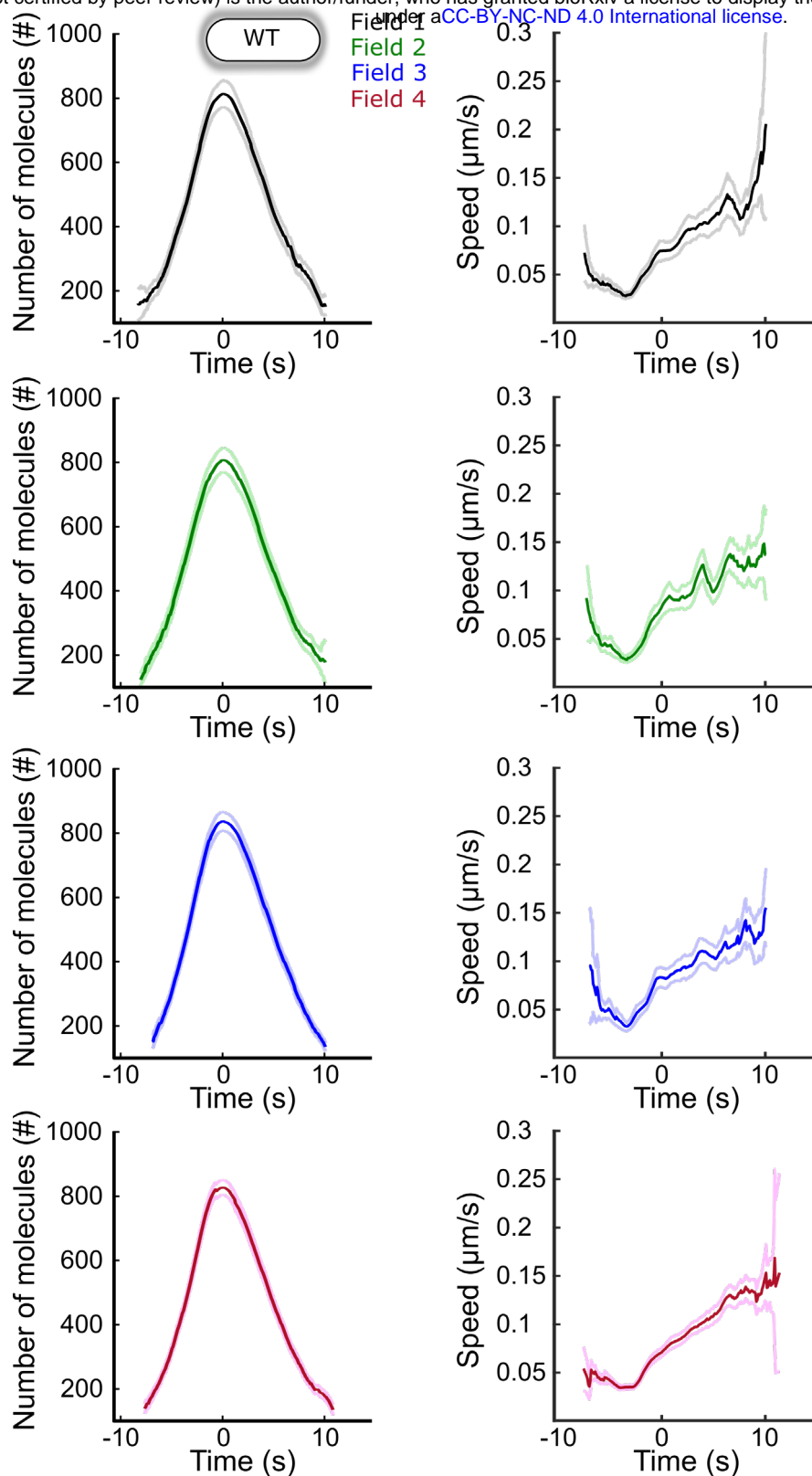


Figure 1 Supplement 1: Separate plots for the data from each field of view in panels 1F and 1G. Each curve with a dark color represents the average of several endocytic events from a different field of view of the same sample ($N \geq 64$), and the light colors are the 95% confidence intervals. For each average curve, the peak value

bioRxiv preprint doi: <https://doi.org/10.1101/342030>; this version posted November 23, 2020. The copyright holder for this preprint (which was not certified by peer review) is the author/funder, who has granted bioRxiv a license to display the preprint in perpetuity. It is made available under aCC-BY-NC-ND 4.0 International license.

corresponds to time 0 sec, when vesicles scission happens. The numbers of endocytic events used in each curve are given in Supplemental Table 2.

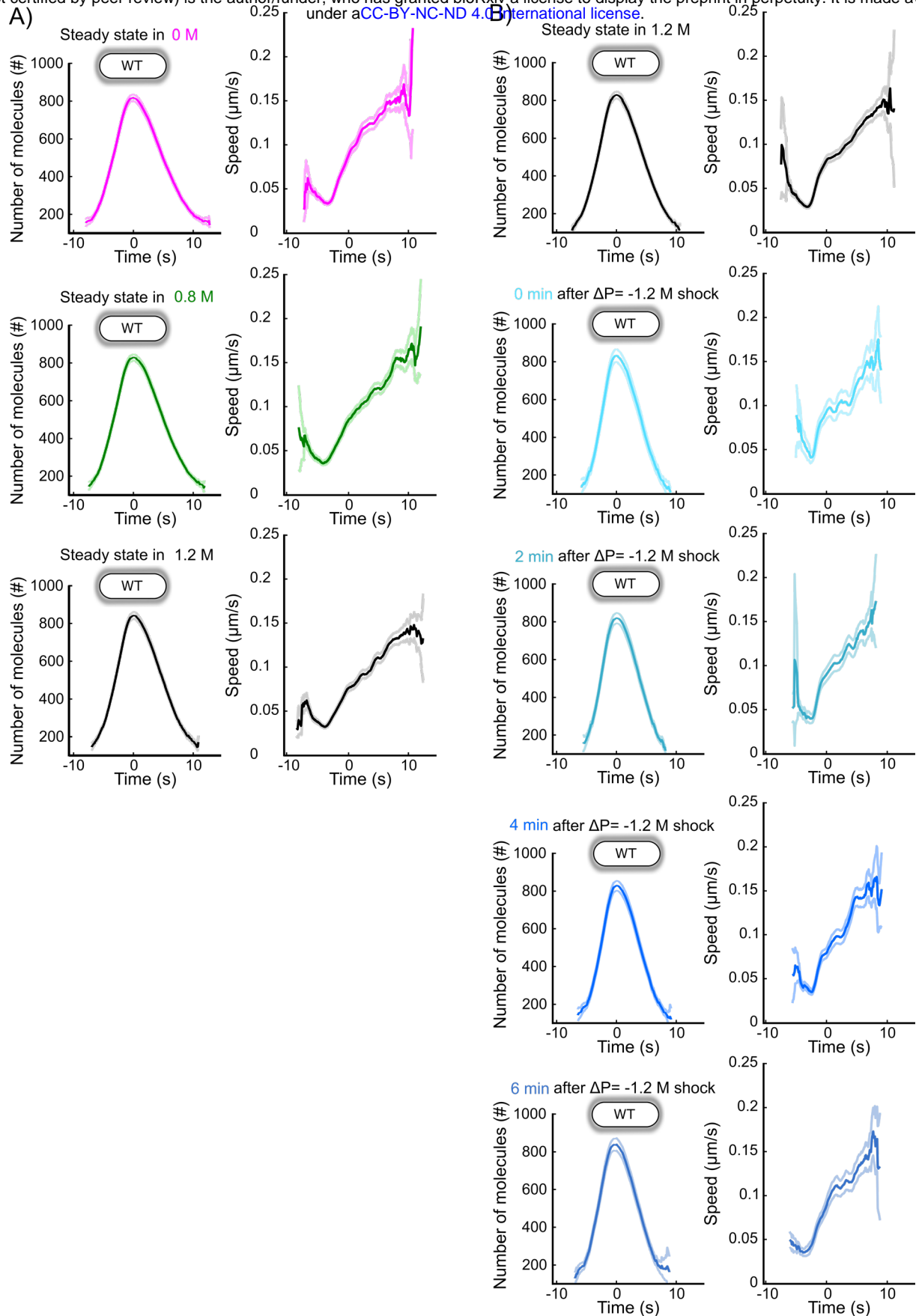


Figure 2 Supplement 1: Separate plots for each condition in Figures 2B (A) and 2F (B). A) Number of molecules (left panel) and speed (right panel) of Fim1p-mEGFP in wild-type walled cells at steady state in media supplemented with different sorbitol

concentrations ($N \geq 388$) (Figure 2B). The numbers of endocytic events used in each curve are given in Supplemental Table 3. E) Number of molecules (left panel) and speed (right panel) of Fim1p-mEGFP for wild-type walled cells initially at steady state in 1.2 M sorbitol and after an acute osmotic shock of $\Delta P = -1.2$ M. Black: steady state in 1.2 M sorbitol; light to dark blue (from top to bottom rows): 0 min, 2 min, 4 min, and 6 min after the acute hypotonic shock ($N \geq 103$) (Figure 2F). The numbers of endocytic events used in each curve are given in Supplemental Table 4. (A) and (B): dark colors: average; light colors: average \pm 95% confidence interval.

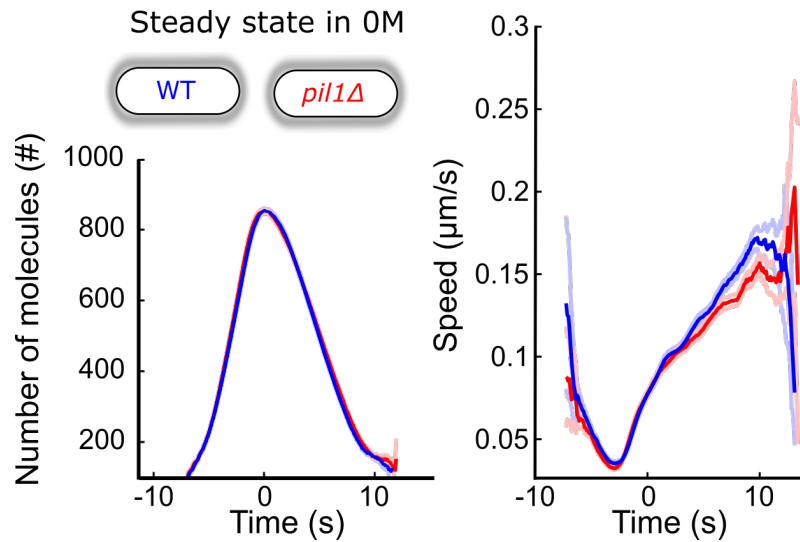


Figure 3 Supplement 1: The number of molecules (left panel) and speed (right panel) of Fim1p-mEGFP at CME sites in wild-type (blue, N=1773) and *pil1Δ* (red, N=1884) walled cells at steady state in EMM5S without sorbitol are identical (same data as Figures 2B and 3B). Dark colors: average, light colors: average \pm 95% confidence interval.

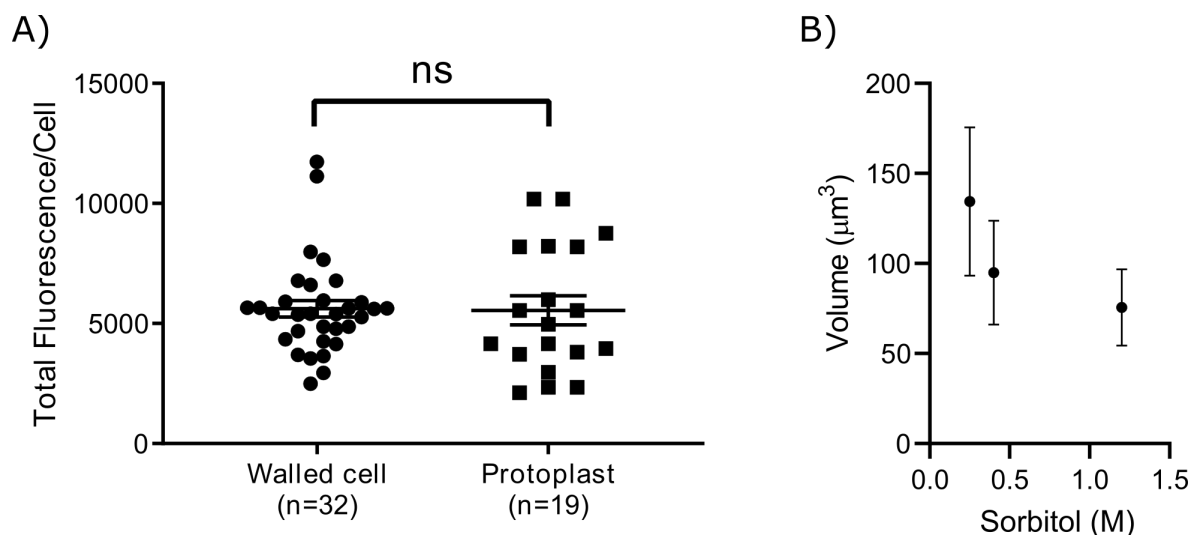


Figure 4 Supplemental 1: A) The total amount of Pil1-mEGFP in walled cells and protoplasts are not significantly different (Mann-Whitney test, $P=0.65$). Bars: mean and standard error of the mean. B) Protoplasts volume at steady state in 0.25 M ($N=26$), 0.4 M ($N=34$) and 1.2 M ($N=39$) sorbitol (same cells were used as in Figure 4C). Error bars: standard deviations.

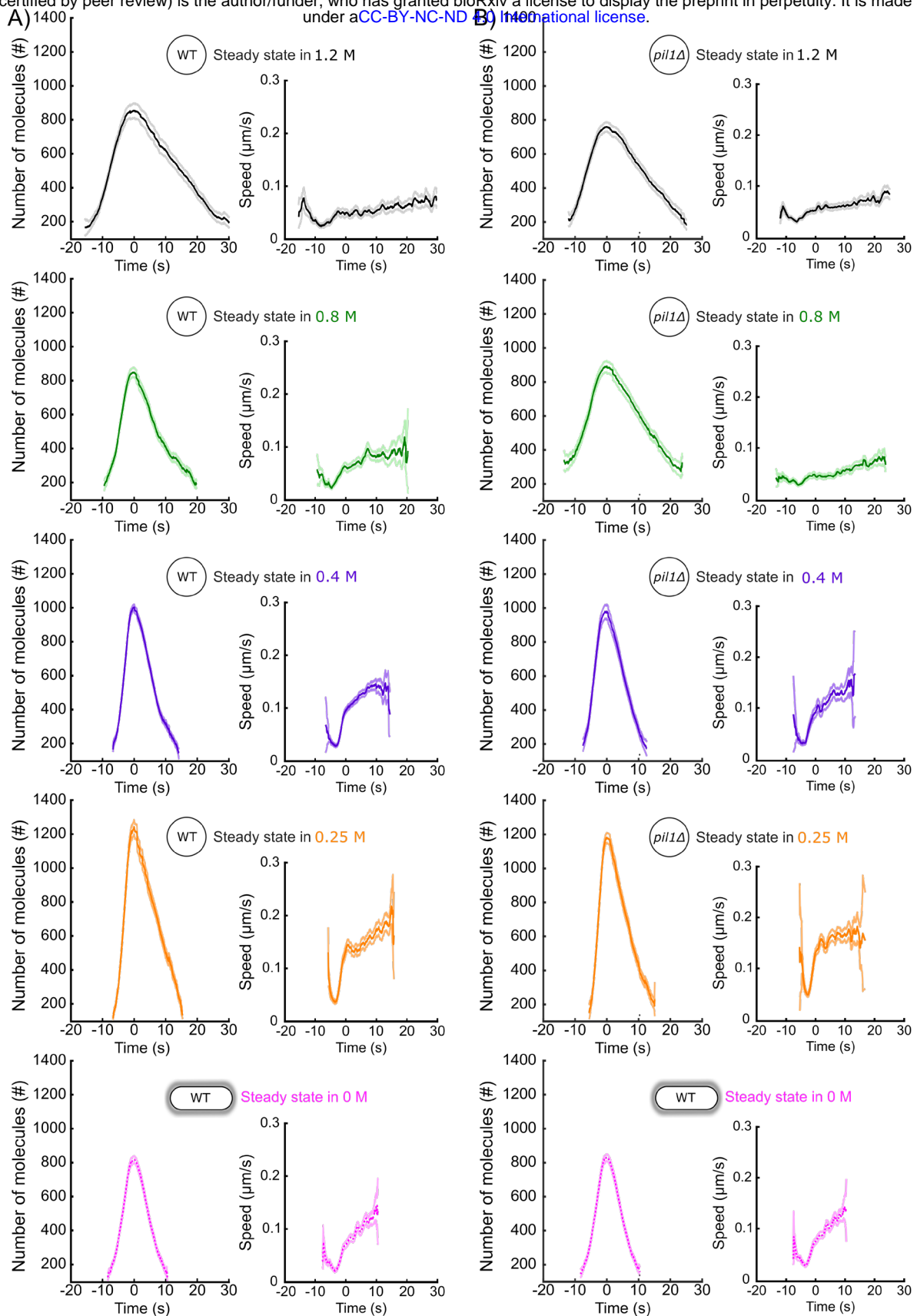


Figure 4 Supplemental 2: Separate plots for each condition in Figures 4F (A) and 4G (B). A) and B) Number of molecules (left panels) and speed (right panels) of Fim1p-mEGFP for wild-type (A) and *pil1Δ* (B) protoplasts at steady state in different sorbitol concentrations. Orange: 0.25 M; purple: 0; green: 0.8 M; black: 1.2 M. Dark

bioRxiv preprint doi: <https://doi.org/10.1101/342030>; this version posted November 23, 2020. The copyright holder for this preprint (which was not certified by peer review) is the author/funder, who has granted bioRxiv a license to display the preprint in perpetuity. It is made available

under a [CC-BY-NC-ND 4.0 International license](#).
colors: average; light colors: average \pm 95% confidence interval (N \geq 143). Fuschia dotted curves: wild-type walled cells at steady state in 0 M sorbitol (same as Figure 3B). The numbers of endocytic events used in each curve are given in Supplemental Table 7.

WT

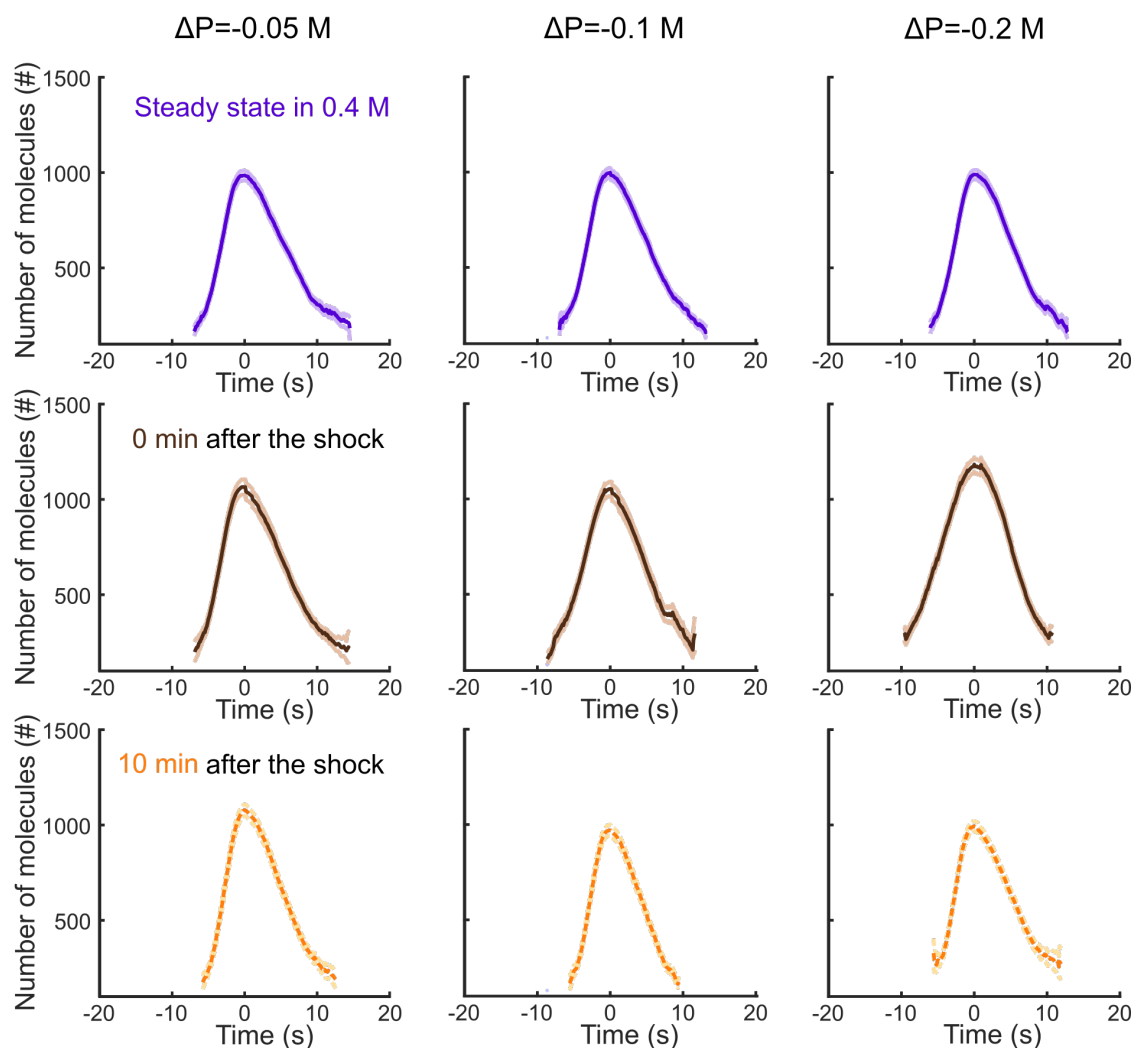


Figure 5 Supplement 1: Separate plots for each condition shown in Figure 5C. Number of Fim1p-mEGFP molecules in wild-type protoplasts at steady-state in 0.4 M sorbitol (purple), 0 min (brown) and 10 min (orange) after an hypotonic shock of $\Delta P = -0.05$ M (left panels), $\Delta P = -0.1$ M (middle panels) and $\Delta P = -0.2$ M (right panels), $N \geq 95$. The speeds of Fim1p-mEGFP for each condition are shown in Figure 5 Supplements 3. The numbers of endocytic events used in each curve are given in Supplemental Table 8. Dark colors: average, light colors: average \pm 95% confidence interval.

pil1Δ

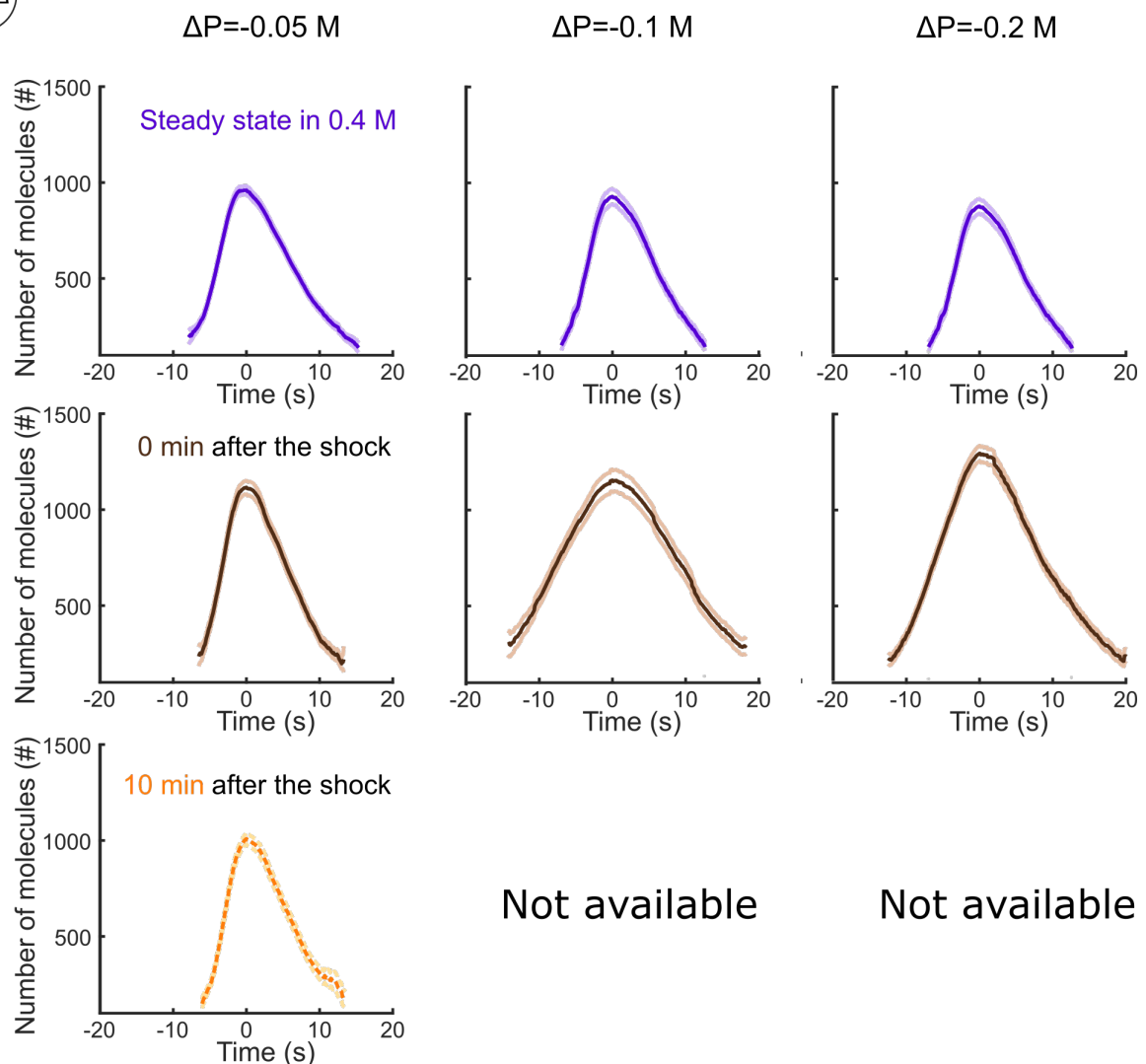
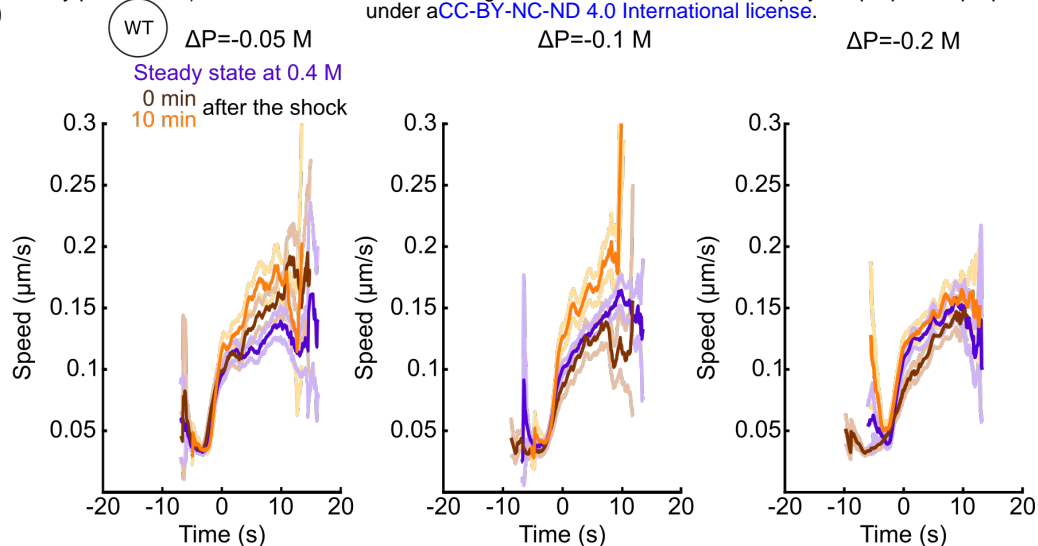


Figure 5 Supplement 2: Separate plots for each condition shown in Figure 5F. Number of Fim1p-mEGFP molecules in *pil1Δ* protoplasts at steady-state in 0.4 M sorbitol (purple), 0 min (brown) and 10 min (orange) after an hypotonic shock of $\Delta P = -0.05$ M (left panels), $\Delta P = -0.1$ M (middle panels) and $\Delta P = -0.2$ M (right panels), $N \geq 95$. The speeds of Fim1p-mEGFP for each condition are shown in Figure 5 Supplements 4. The numbers of endocytic events used in each curve are given in Supplemental Table 8. Note that the large majority of *pil1Δ* protoplasts were too damaged or dead 2 minutes after hypotonic shocks larger than or equal to $\Delta P = -0.1$ M to allow us to track enough endocytic events and produce a curve (Figures 6B and C, Figure 6 Supplement 1). Dark colors: average, light colors: average \pm 95% confidence interval.

A)



B)

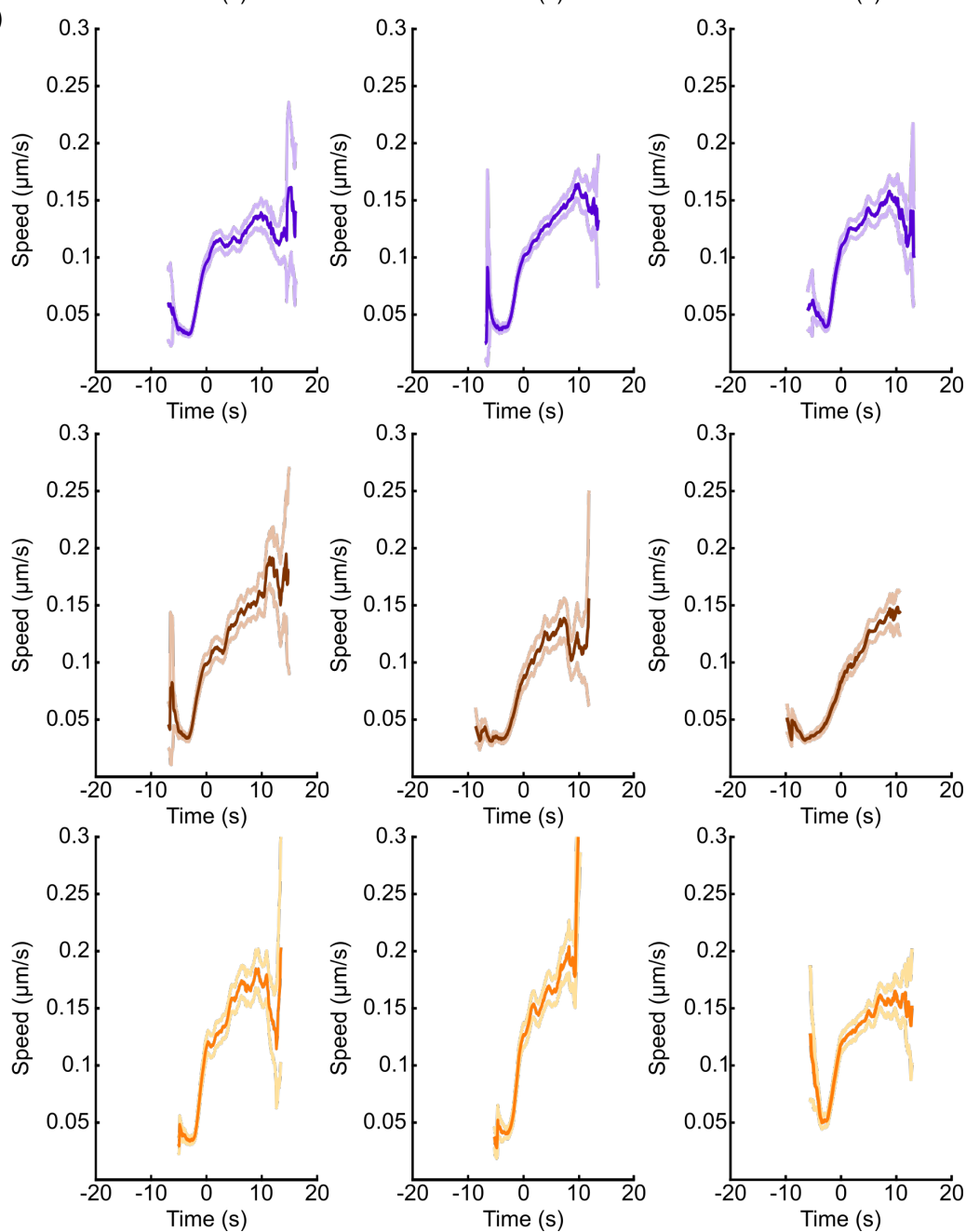
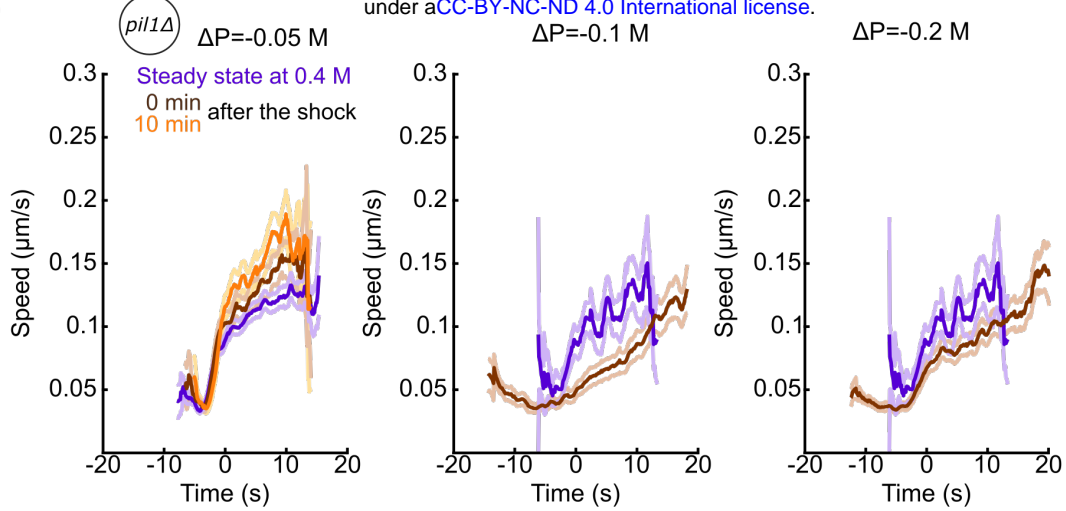


Figure 5 Supplement 3: A) Speed of Fim1p-mEGFP in wild-type protoplasts at steady-state in 0.4 M sorbitol (purple), 0 min (brown) and 10 min (orange) after an hypotonic shock of $\Delta P = -0.05$ M (left panels), $\Delta P = -0.1$ M (middle panels) and $\Delta P = -0.2$ M (right panels). B) Separate plots for each condition shown in panel A. (A and B) The same endocytic events as the ones used in Figure 5C have been used to generate these plots. The numbers of endocytic events used in each curve are given in Supplemental Table 8. Dark colors: average, light colors: average \pm 95% confidence interval.

A)



B)

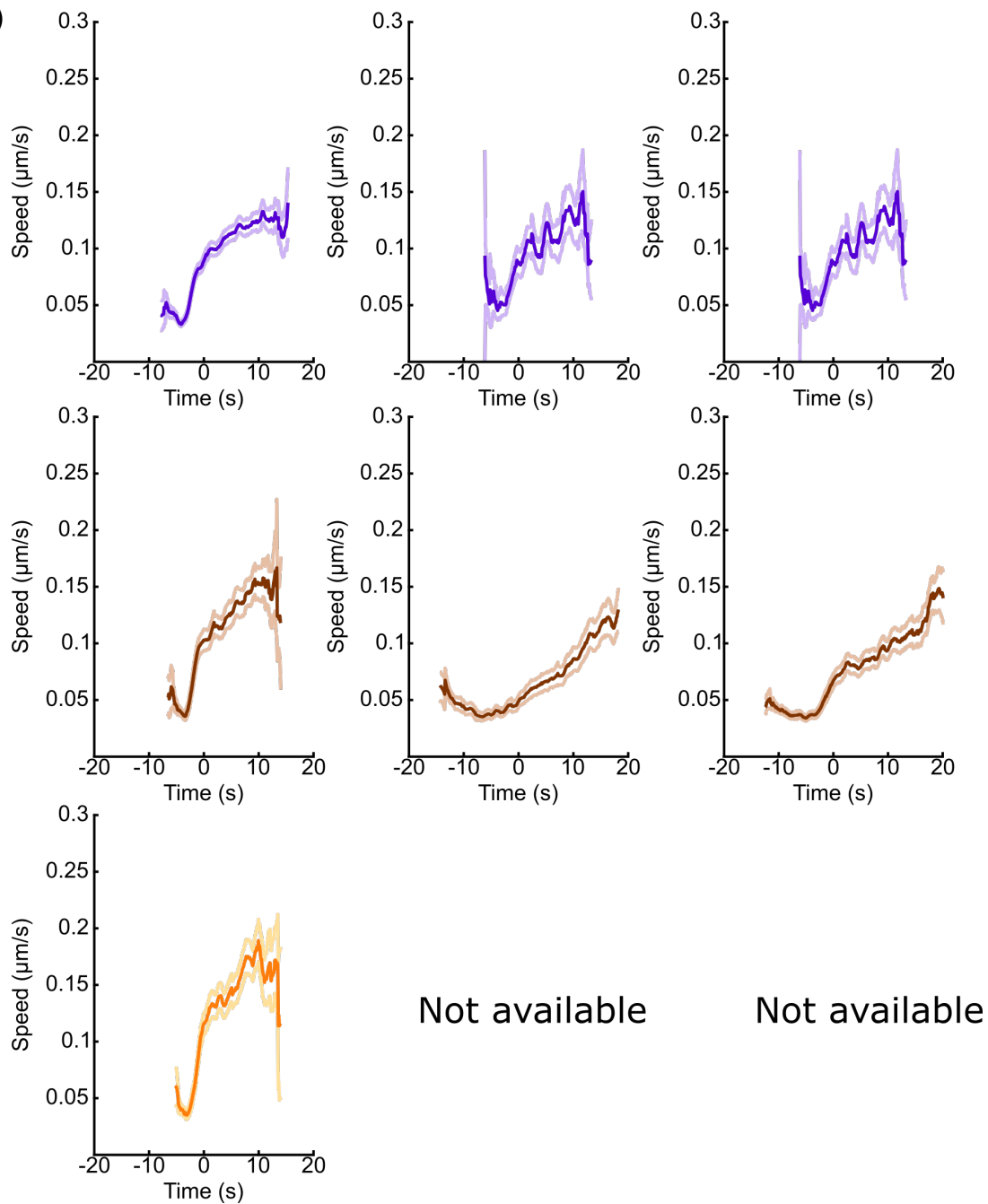


Figure 5 Supplement 4: A) Speed of Flm1p-mEGFP in *pil1Δ* protoplasts at steady-state in 0.4 M sorbitol (purple), 0 min (brown) and 10 min (orange) after an hypotonic shock of $\Delta P = -0.05$ M (left panels), $\Delta P = -0.1$ M (middle panels) and $\Delta P = -0.2$ M (right panels). B) Separate plots for each condition shown in panel A. (A and B) The same endocytic events as the ones used in Figure 5F have been used to generate these plots. The numbers of endocytic events used in each curve are given in Supplemental Table 8. Dark colors: average, light colors: average \pm 95% confidence interval.

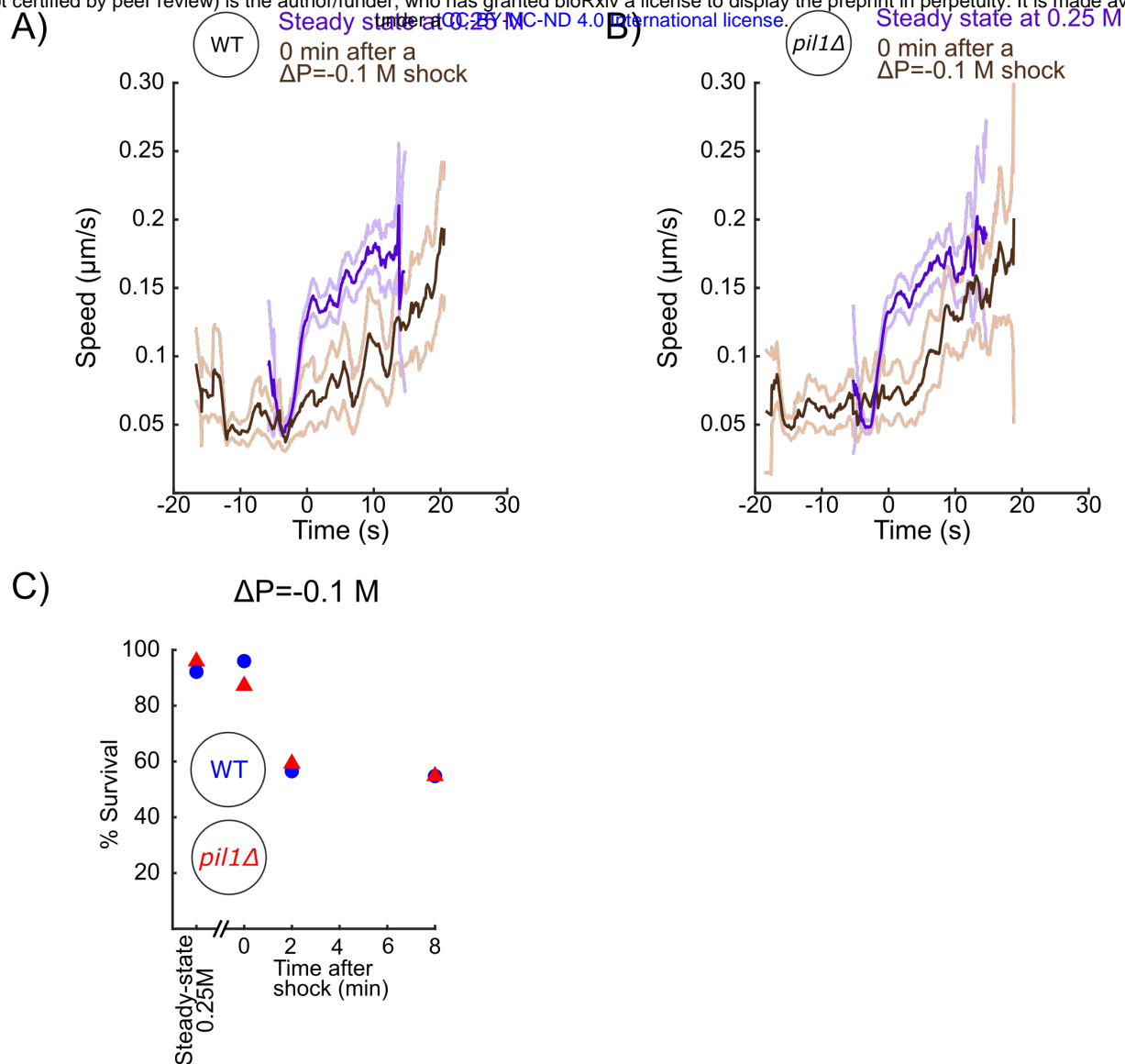
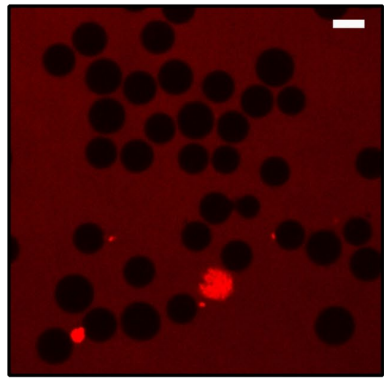


Figure 5 Supplement 5: (A and B) Speed of Fim1p-mEGFP at CME sites for wild-type (A) and *pil1Δ* (B) protoplasts at steady-state in 0.25 M sorbitol (purple) and immediately (0 min) after (brown) a hypotonic shock of $\Delta P = -0.1$ M. The same endocytic events as the ones used in Figure 5H (A) and 5I (B) have been used to generate these plots. The numbers of endocytic events used in each curve are given in Supplemental Table 10. Dark colors: average, light colors: average \pm 95% confidence interval. C) Percentage of wild-type (blue dots) and *pil1Δ* (red triangles) protoplasts that are alive in fields of view used for analysis, at steady-state in 0.25 M sorbitol, and after a $\Delta P = -0.1$ M hypotonic shock.

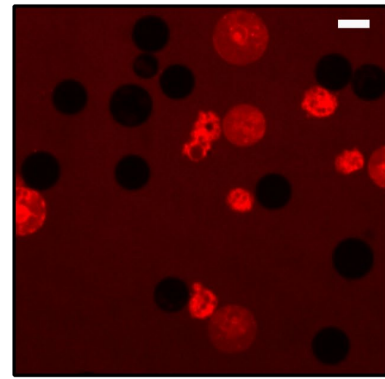
A)

WT



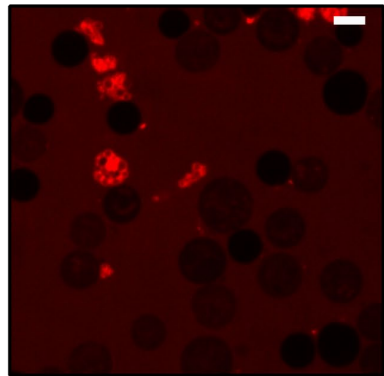
Steady-state 0.4 M

8 minutes after a $\Delta P = -0.1$ M shock



B)

pil1 Δ



Steady-state 0.4 M

8 minutes after a $\Delta P = -0.1$ M shock

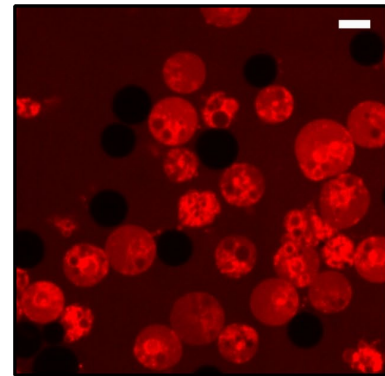


Figure 6 Supplement 1: A) and B) Typical fields of view of wild-type (A) and *pil1* Δ (B) protoplasts at steady state in 0.4 M sorbitol (left panel) and 8 minutes (right panel) after a $\Delta P = -0.1$ M hypotonic shock. Cells are considered alive if they do not contain any red fluorescence from the sulforhodamin B dye. Scale bar: 5 μ m.

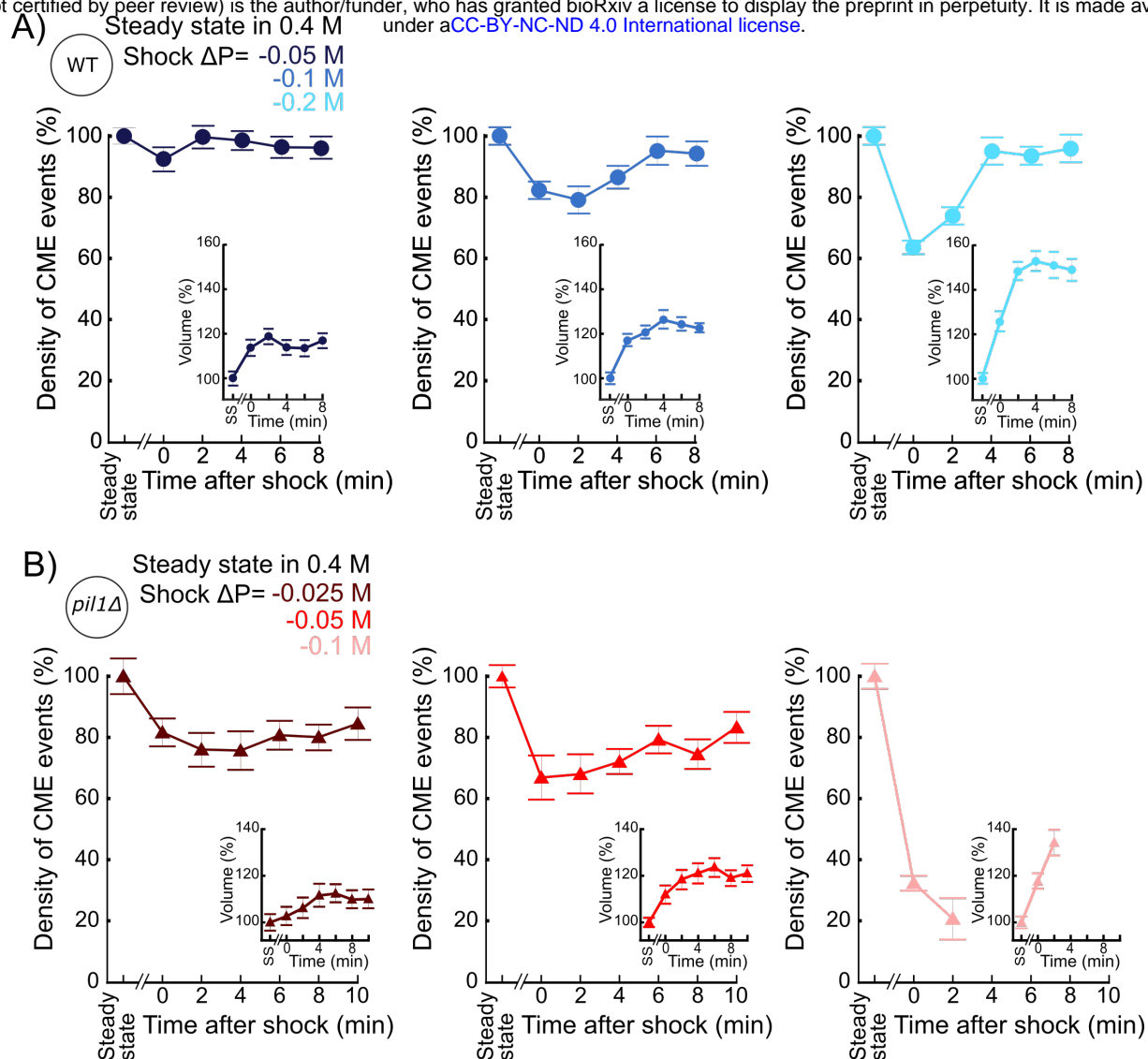


Figure 7 – Supplement 1: Separate plots for each condition shown in Figure 7A and B. A) Temporal evolution of density of endocytic events (average number of endocytic events at a given time in a cell divided by the cell length) in wild-type protoplasts initially at steady state in 0.4 M sorbitol and after an acute hypotonic shock of $\Delta P = -0.05$ M (dark blue, $N_{\text{cell}} \geq 102$), $\Delta P = -0.1$ M (blue, $N_{\text{cell}} \geq 54$) and $\Delta P = -0.2$ M (light blue, $N_{\text{cell}} \geq 83$). B) Same as (A) but with *pil1Δ* protoplasts and hypotonic shocks of $\Delta P = -0.025$ M (dark red, $N_{\text{cell}} \geq 70$), $\Delta P = -0.05$ M (red, $N_{\text{cell}} \geq 103$) and $\Delta P = -0.1$ M (light red, $N_{\text{cell}} \geq 78$). (A) and (B) insets: relative volume increase after the hypotonic shocks (the volume at steady state is used as a reference). The number of cells used for each condition and each time point is given in Supplemental Table 11. The number of cells measured in the insets are the same as in the main figures. (A) and (B): error bars are standard errors of the mean. The number of cells used for each condition and each time point is given in Supplemental Table 13.

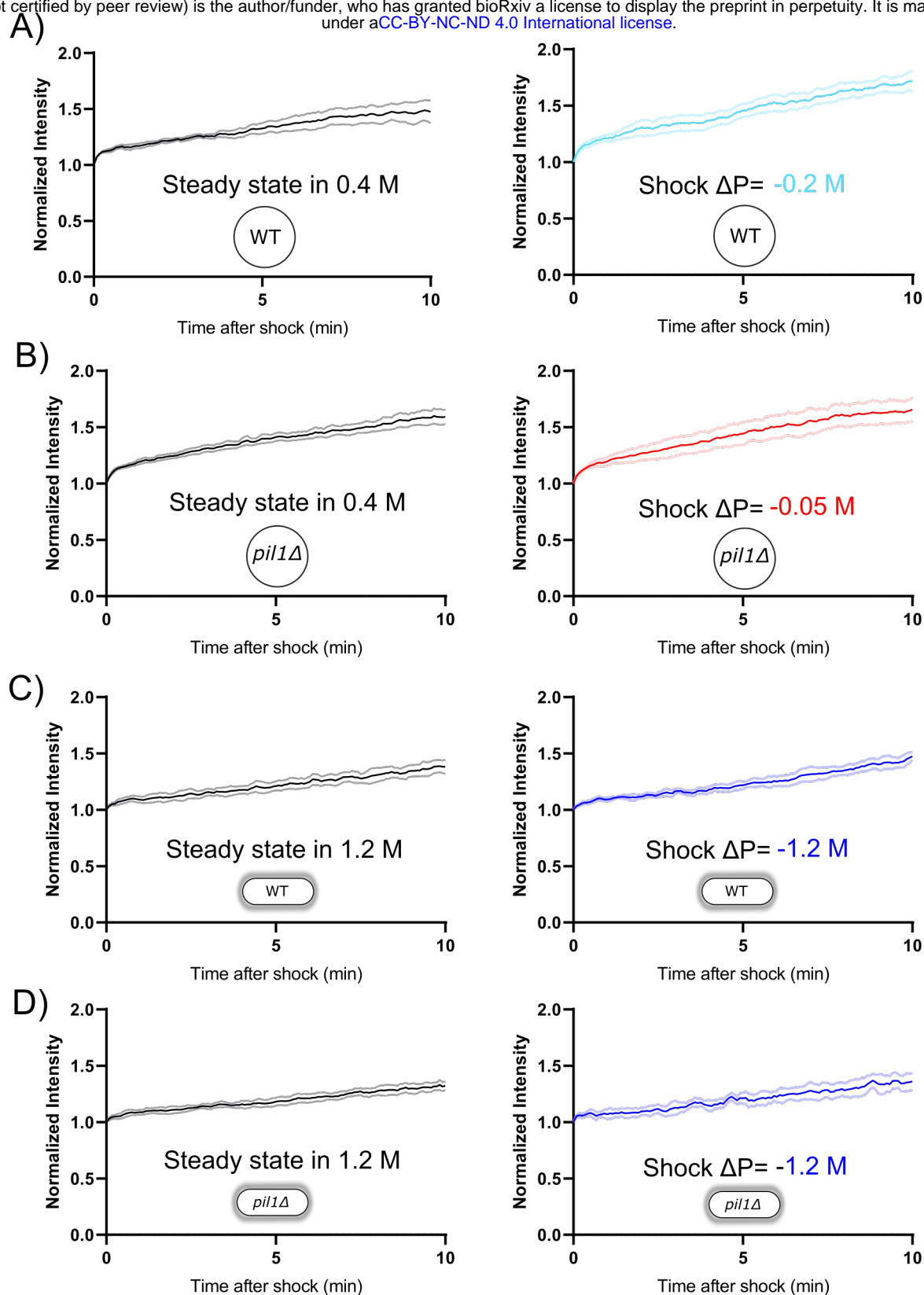


Figure 8 – Supplement 1: Separate plots for each condition in Figure 8. Rates of exocytosis at steady state and after hypotonic shocks. A) and B) The exocytic rate of wild-type and *pil1* Δ protoplasts increases after a $\Delta P = -0.2$ M (black, before shock, $N_{\text{cells}}=20$; light blue, after shock, $N_{\text{cells}}=37$; 4 replicates each) and $\Delta P = -0.05$ M (black, before shock, $N_{\text{cells}}=44$; red, after shock, $N_{\text{cells}}=60$; 4 replicates each) acute hypotonic

shocks, respectively. Before time 0 min, all protoplasts were at steady-state in 0.4 M sorbitol. C) and D) The exocytic rate of wild-type walled cells is not changed after a $\Delta P = -1.2$ M acute hypotonic shock (black, before shock, $N_{\text{cells}} = 79$; blue, after shock, $N_{\text{cells}} = 68$; 3 replicates each). The exocytic rate of *pil1* Δ walled cells does not change significantly in the same conditions (black, before shock, $N_{\text{cells}} = 60$; blue, after shock, $N_{\text{cells}} = 96$; 3 replicates each). All walled cells were at steady-state in 1.2 M sorbitol before time 0 min. (A)-(E) Dark color: mean; light color: standard error of the mean.

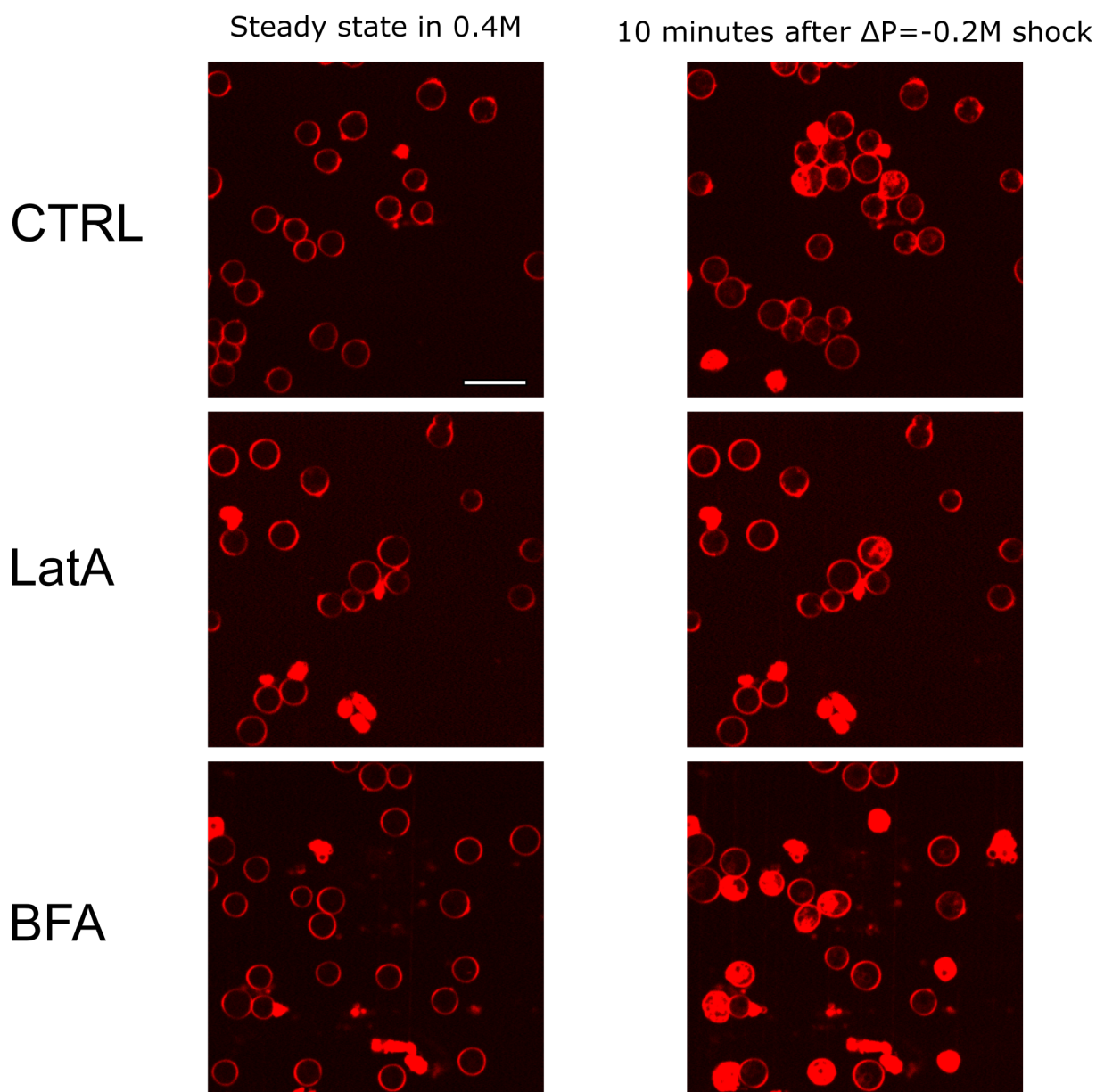


Figure 9 Supplemental 1: Typical fields of view of *pil1* Δ protoplasts at steady state in 0.4 M sorbitol (left panel) and 10 minutes (right panel) after a $\Delta P = -0.2$ M hypotonic shock. First row: control, second row: latrunculin A, third row: Brefeldin A. Cells are considered dead if they contain large amounts of intracellular red fluorescence from the FM4-64 dye, which is the consequence of a rupture of the plasma membrane. Scale bar: 10 μm .

Supplemental tables

Supplemental Table 1: Yeast strains

Strain	Genotype	Mating type
SpJB57	fim1-mEGFP-NatMX6 ade6-M216 his3- Δ 1 leu1-32 ura4- Δ 18	h+
SpJB204	pil1-mEGFP-kanMX6 ade6-M216 his3- Δ 1 leu1-32 ura4- Δ 18	h-
SpJB234	pil1 Δ fim1-mEGFP-NatMX6 ade6-M216 his3- Δ 1 leu1-32 ura4- Δ 18	h-
SpJB566	mScarlet-l-end4 mEGFP-fim1 fex1 Δ fex2 Δ ade6-M216 his3-D1 leu1-32 ura4-D18	h-

Supplemental Table 2: Number of endocytic events used to generate Figures 1F and 1G

Field of view	Number of tracks
Field 1	64
Field 2	79
Field 3	91
Field 4	202

Supplemental Table 3: Number of endocytic events used to generate Figure 2B

Sorbitol concentration	Number of tracks
0 M	388
0.8 M	454
1.2 M	451

Supplemental Table 4: Number of endocytic events used to generate Figure 2E

Time point	Number of tracks
Steady state	354
0 min	103
2 min	169
4 min	190
6 min	153

Supplemental Table 5: Number of endocytic events used to generate Figure 3B

Sorbitol concentration	Number of tracks
0 M	342
0.8 M	516
1.2 M	514

Supplemental Table 6: Number of endocytic events used to generate Figure 3D

Time point	Number of tracks
Steady state	583
0 min	176
2 min	145
4 min	326

Supplemental Table 7: Number of endocytic events used to generate Figures 4F and 4G

Sorbitol concentration	Number of tracks WT cells	Number of tracks <i>pil1Δ</i> cells
Protoplasts in 1.2 M	143	203
Protoplasts in 0.8 M	151	184
Protoplasts in 0.4 M	682	166
Protoplasts in 0.25 M	395	370
WT walled cells in 0M	234	300

Supplemental Table 8: Number of endocytic events used to generate Figures 5C and 5F

$\Delta P = -0.05M$

Time point	Number of tracks WT cells	Number of tracks <i>pil1</i> Δ cells
Steady state in 0.4M	279	429
0 min after $\Delta P = -0.05M$	193	183
10 min after $\Delta P = -0.05M$	182	206

$\Delta P = -0.1M$

Time point	Number of tracks WT cells	Number of tracks <i>pil1</i> Δ cells
Steady state in 0.4M	413	95
0 min after $\Delta P = -0.1M$	190	215
10 min after $\Delta P = -0.1M$	186	\emptyset

$\Delta P = -0.2M$

Time point	Number of tracks WT cells	Number of tracks <i>pil1</i> Δ cells
Steady state in 0.4M	269	95
0 min after $\Delta P = -0.2M$	396	373
10 min after $\Delta P = -0.2M$	309	\emptyset

Supplemental Table 9: Number of endocytic events used to generate Figure 5D and 5G

Time point	Number of tracks WT cells
Steady state in 0.4M	269
0 min after $\Delta P = -0.2M$	396
2 min after $\Delta P = -0.2M$	124
4 min after $\Delta P = -0.2M$	127
6 min after $\Delta P = -0.2M$	178
8 min after $\Delta P = -0.2M$	255
10 min after $\Delta P = -0.2M$	309

Time point	Number of tracks <i>pil1Δ</i> cells
Steady state in 0.4M	429
0 min after $\Delta P = -0.05M$	183
2 min after $\Delta P = -0.05M$	188
4 min after $\Delta P = -0.05M$	162
6 min after $\Delta P = -0.05M$	193
8 min after $\Delta P = -0.05M$	197
10 min after $\Delta P = -0.05M$	206

Supplemental Table 10: Number of endocytic events used to generate Figures 5H and 5I

Time point	Number of tracks WT cells	Number of tracks <i>pil1Δ</i> cells
Steady state in 0.25M	226	182
0 min after $\Delta P = -0.1 M$	75	67

Supplemental Table 11: Number of cells used to generate Figures 7A and 7B

$\Delta P = -0.025M$

Time point	Number of cells WT cells	Number of cells <i>pil1Δ</i> cells
Steady state in 0.4M	∅	99
0 min after $\Delta P = -0.025 M$	∅	100
2 min after $\Delta P = -0.025 M$	∅	71
4 min after $\Delta P = -0.025 M$	∅	70
6 min after $\Delta P = -0.025 M$	∅	98
8 min after $\Delta P = -0.025 M$	∅	118
10 min after $\Delta P = -0.025 M$	∅	96

$\Delta P = -0.05M$

Time point	Number of cells WT cells	Number of cells <i>pil1Δ</i> cells
Steady state in 0.4M	172	263
0 min after $\Delta P = -0.05 M$	102	106
2 min after $\Delta P = -0.05 M$	117	111
4 min after $\Delta P = -0.05 M$	114	106
6 min after $\Delta P = -0.05 M$	113	103
8 min after $\Delta P = -0.05 M$	124	123
10 min after $\Delta P = -0.05 M$	∅	104

$\Delta P = -0.1 M$

Time point	Number of cells WT cells	Number of cells <i>pil1</i> Δ cells
Steady state 0.4M	127	151
0 min after $\Delta P = -0.1 M$	62	125
2 min after $\Delta P = -0.1 M$	70	78
4 min after $\Delta P = -0.1 M$	78	\emptyset
6 min after $\Delta P = -0.1 M$	62	\emptyset
8 min after $\Delta P = -0.1 M$	54	\emptyset

$\Delta P = -0.2 M$

Time point	Number of cells WT cells	Number of cells <i>pil1</i> Δ cells
Steady state 0.4M	146	\emptyset
0 min after $\Delta P = -0.2 M$	149	\emptyset
2 min after $\Delta P = -0.2 M$	158	\emptyset
4 min after $\Delta P = -0.2 M$	83	\emptyset
6 min after $\Delta P = -0.2 M$	107	\emptyset
8 min after $\Delta P = -0.2 M$	83	\emptyset

Supplemental Table 12: Number of cells used to generate Figure 7C

Time point	Number of cells WT cells	Number of cells <i>pil1</i> Δ cells
Steady state 1.2M	62	119
0 min after $\Delta P = -1.2 M$	82	69
2 min after $\Delta P = -1.2 M$	77	44
4 min after $\Delta P = -1.2 M$	67	67
6 min after $\Delta P = -1.2 M$	66	\emptyset

Supplemental Table 13: Number of cells used to generate Figure 7D

Sorbitol Concentration	Number of cells WT cells	Number of cells <i>pil1</i> Δ cells
Steady state in 0 M	240	188
Steady state in 0.8 M	103	105
Steady state in 1.2 M	159	183
Steady state in 2 M	161	80